UNIVERSITY OF OKLAOMA
GRADUATE COLLEGE

ACTIVATION OF INTERFERON THROUGH GLYCATED CHITOSAN ADMINISTRATION

A THESIS

SUBMITTED TO THE GRADUATE FACULTY

in partial fulfillment of the requirements for the

Degree of

MASTER OF SCIENCE

By

MALAYNA UNKEL
Norman, Oklahoma
2024

ACTIVATION OF INTERFERON THROUGH GLYCATED CHITOSAN ADMINISTRATION

A THESIS APPROVED FOR THE
STEPHENSON SCHOOL OF BIOMEDICAL ENGINEERING

BY THE COMMITTEE CONSISTING OF

Dr. Wei R. Chen, Chair

Dr. Handan Acar

Dr. Qinggong Tang

Acknowledgment

I first want to thank Dr. Wei R. Chen, my Principal Investigator, for his guidance and for taking a chance on me. Your support in my research and other academic endeavors has been very much appreciated.

To my defense committee members, Dr. Handan Acar and Dr. Qinggong Tang, thank you for lending your time and your feedback.

Further thanks go to my lab colleagues who have contributed invaluably to my work. Trisha Valerio for her patience and support, Jacob Adams for his assistance, Coline Furrer for her advice, Vinit Sheth for his disposition, and Kaili Liu for his expertise.

To Dr. Ashley Hoover, who was gracious enough to extend her help and lend her expertise, I also express my gratitude. This project would not have been possible without you.

Finally, to my family, and especially my parents, I would not be the person I am today without you. None of this would have been possible without you shaping me to get here. I am endlessly thankful for your love and support.

Table of Contents

Abstract

N-dihydrogalactochitosan (GC) is a novel immunoadjuvant with unique physiochemical properties that poses significant improvements upon its parent molecule, chitosan. Its potent immune stimulation properties make it promising in the world of vaccinations, with already proven reduction of morbidity in COVID studies. The key to generating immunity against intracellular pathogens is to generate a type I/II interferon (IFN) response. GC stimulates the desired IFN responses while other currently used adjuvants such as MF-59 often fail to do so. For comparison purposes, the immune response specific to GC stimulation needs to be understood. It has been previously demonstrated that application of GC in combination with photothermal therapy reduces mortality in cancer treatment studies. Furthermore, intranasal application of GC in combination with recombinant viral proteins has reduced COVID-19 mortality in mice. The fundamental question remains: Is GC acting as a physical barrier, or is GC stimulating a local type I IFN response which in turn activates antiviral pathways in the respiratory epithelium? Building on previously found GC immune activations, now presented are the results of gene activation and interferon activation in *in vivo* studies over time. This provides insight into the specific mechanisms by which GC succeeds at inducing anti-tumor and anti-viral immunological responses.

Keywords: glycated chitosan (GC); type I interferon response; immunoadjuvant; anti-tumor and anti-viral immune response

Chapter 1

Introduction

1.1 Immunostimulants/Immunoadjuvants

Immunostimulants are substances that strengthen the body's immune responses to protect against pathogens (Esha Bala, 2019). Immunoadjuvants, a subset of immunostimulants, are substances meant to enhance the immune response when used in conjugation with other inoculation substances (e.g., vaccines and recombinant proteins) (Zhou e. a., 2015). The benefit is that they are able to enhance the body's natural defense responses, generating an even stronger reaction to create protection against pathogens of all kinds (McNab, 2015). This makes them useful in vaccine formulations, and they are also coming into play with much promise in the world of cancer therapeutics. In both of these application fields, immunoadjuvants have shown enhanced efficacy. Additionally, both of these applications demand immune interplay for success, so better mechanistic understanding is key to improved therapies (CDC, 2022).

1.2 Glycated Chitosan

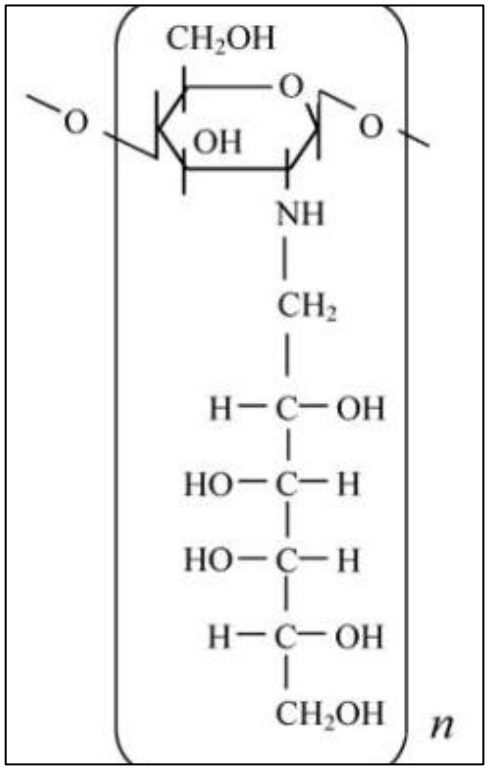

Figure 1: Glycated Chitosan Chemical Structure. *This figure shows the chemical structure of GC, a novel immunoadjuvant derived from parent chitosan.*

N-dihydrogalactochitosan, commonly called glycated chitosan (GC), is a novel immunostimulant to improve upon the effects of current adjuvants in cancer combination therapy (**Figure 1**). GC retains the biological properties of its parent molecule chitosan, a commonly used adjuvant (Zhao, 2018) (Carroll, 2016). However, GC also improves the biocompatibility and immune stimulation properties and adds water solubility, making it much more promising for clinical applications (Song, 2009). Additionally, GC has been shown to induce interferon responses that significantly enhance drug efficacy in cancer therapies (Hoover, 2022). When used as an immunoadjuvant, i.e., in combination with antigenic material, GC stimulates the innate response and improves the adaptive response (Li, 2011).

1.3 GC in Laser Immunotherapy

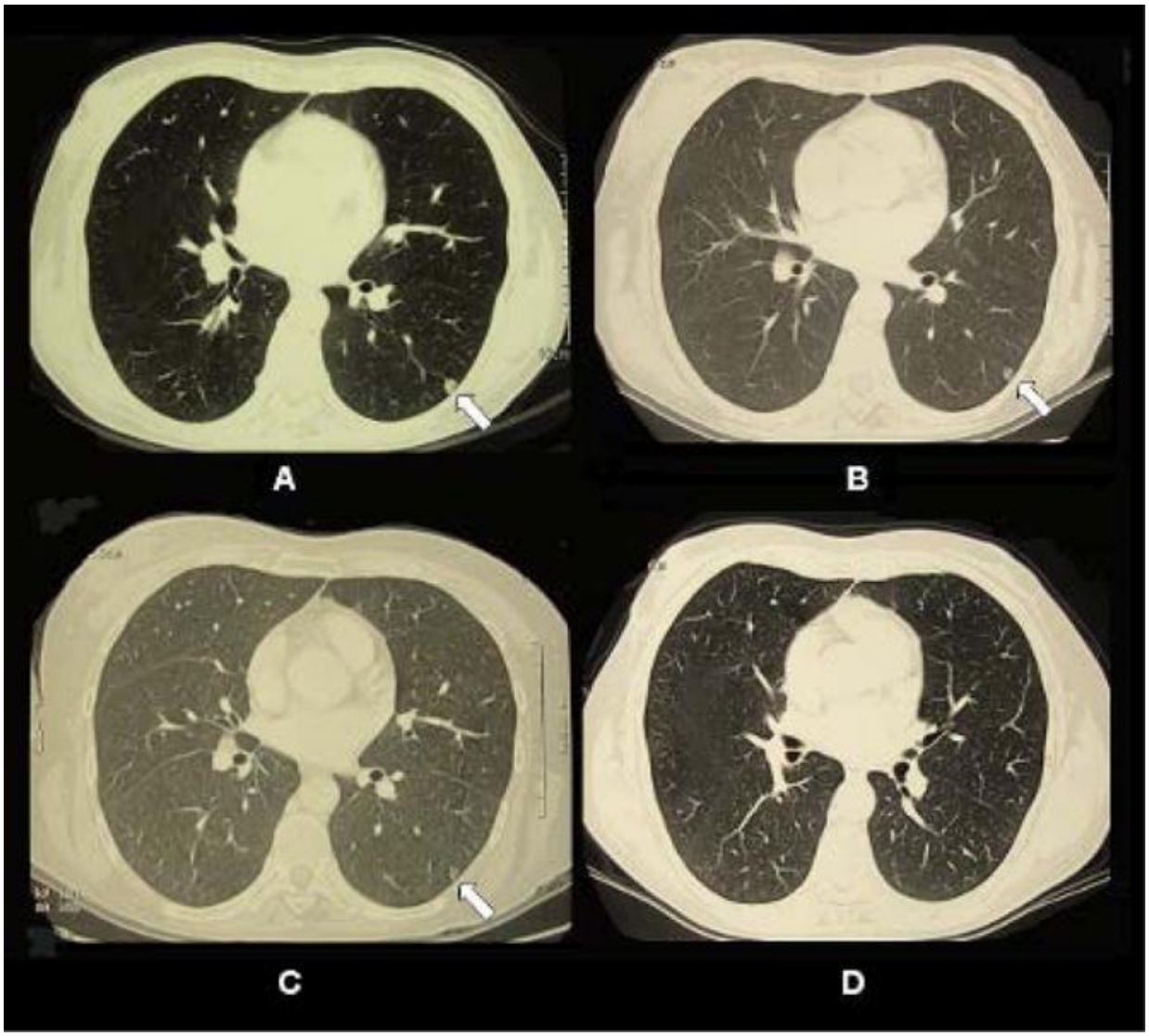

Figure 2: Previous results using LIT. *This figure is from a study that can be found in (Li, 2011). The figure shows CT scans of pulmonary metastatic nodule in the left lung of a late-stage breast cancer patient. The nodule is marked by the arrow in images A-C. It depicts the progression of tumor reduction in response to laser immunotherapy treatment. Image A is at the pre-treatment time point, image B at 1 week-post treatment, image C at 2.5 months post-treatment, and image D at 12 months post-treatment.*

Cancer, which is characterized by uncontrolled cell growth, is often notorious in immune response repression (NIH, 2021). Cancer cells can develop mechanisms by which to evade the body's natural cell destruction mechanisms, allowing for the unchecked proliferation (Cho,

2022). Furthermore, its metastasis– spread to other parts of the body– often means a terminal outcome, with this stage designation accounting for at least 66% of cancer-related deaths (Dillekas, 2019). Traditional treatments often pose the problem of later recurrence. Immunotherapy is an upcoming treatment modality that aims to maximize efficacy by reinitiating the body's own natural defenses. The potential of immunotherapy is the production of memory immune responses (Vatner, 2019). The treatment can produce an immediate fight against primary tumors and metastases by essentially activating the immune response to recognize the cells that have been going unnoticed, and it can later fight against recurrences with memory development. Furthermore, because immunotherapy allows for exploitation of the body's own natural response, thus creating a strong therapy in and of itself, a lower intensity of coupled treatment is required to generate an effective systemic response, making it a safer alternative in many cases.

Laser immunotherapy (LIT) is a novel combination therapy developed for the treatment of cancer of various types (Li, 2011). It entails the application of photothermal therapy followed by an immunoadjuvant drug (Naylor, 2006). GC has been developed as a novel immunoadjuvant for use in this therapy and has showed promising preliminary results in extending survival time (Zhou e. a., 2015). Previous studies have shown that the major immune stimulation in ablation-GC treatment was in fact caused by GC (Zhou, 2018). This combination induced tumor regression of both primary tumors and metastases (Liu, 2022).

1.4 Interferon Response

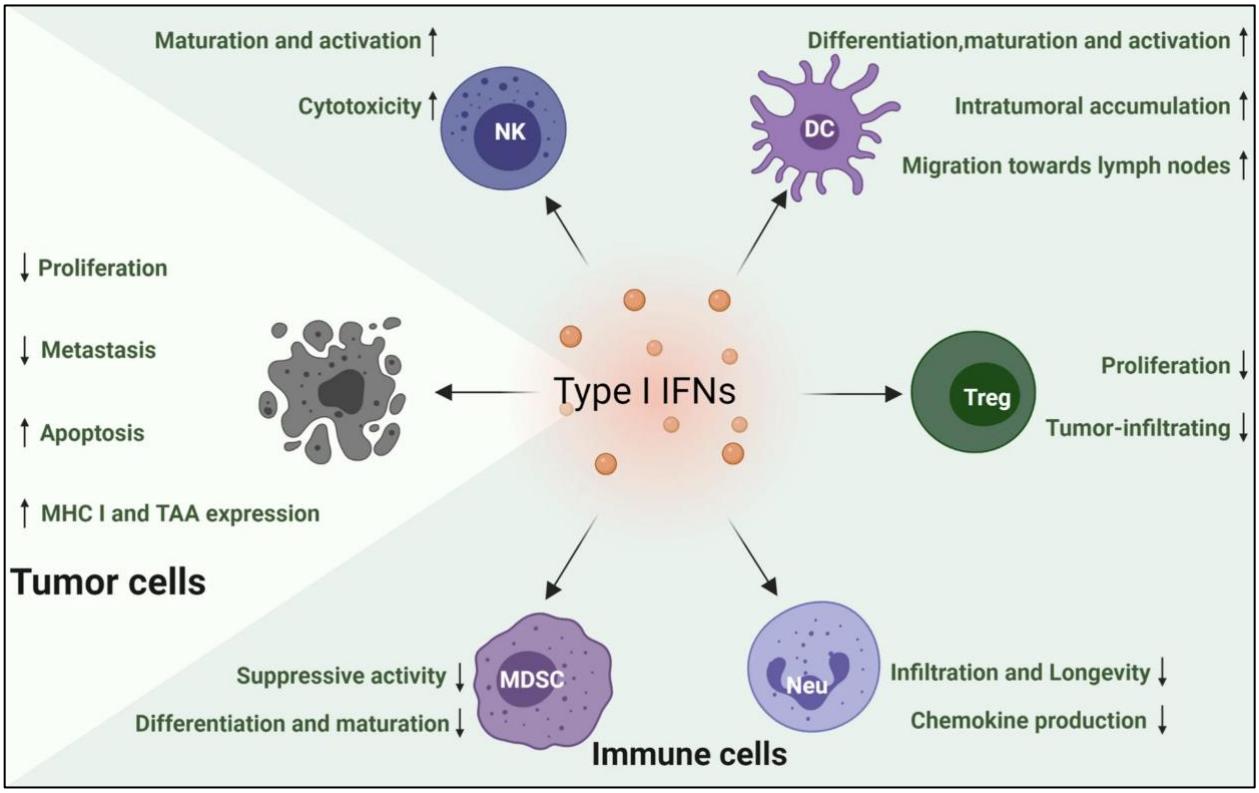

Figure 3: Type I Interferon Effects. *(Yu R. e., 2022) This figure provides an illustration of the effects of type I IFNS in the tumor microenvironment. This gives relevant information for the type I IFN response in the view of the current application of GC, explaining why this response is desired. It shows that Type I IFNs can exhibit upregulation of tumor suppression factors and downregulation of tumor proliferation factors.*

Type I interferons (IFNs) are cytokines important for host defense against viruses as they are rapidly activated during viral infection and can restrict viral replication (Stetson, 2006). They are produced by dendritic cells and macrophages, which are main components in initiating the immune system's innate defense response. Type I IFNs allow protection against pathogens while inducing minimum damage to the host, making their utilization an attractive option for disease therapies (McNab, 2015). Their induction by GC is hypothesized as a main reason for the reduced mortality from COVID after GC administration in work previously done in this lab (see

Appendix D: Previous COVID survival study with GC for results). COVID has in fact been shown to not suppress signaling of type I IFNs, which supports the evidence of GC's IFN production (Shemesh, 2021). Furthermore, IFN-β treatment (a type of IFN-I) was shown in another study to block COVID replication (Lei, 2020).

Additionally, type I IFNs are able to stimulate both the innate and adaptive immune responses, which is paramount in developing an effective response to cancer *in vivo* (Xitvogel, 2015). Specific mechanisms of this activity can be examined in **Figure 3**. Thus, the GC-induced IFN response is further supported by its success in clinical trials of cancer treatment with LIT (Zhou e. a., 2015).

1.5 Intranasal and NALT analysis

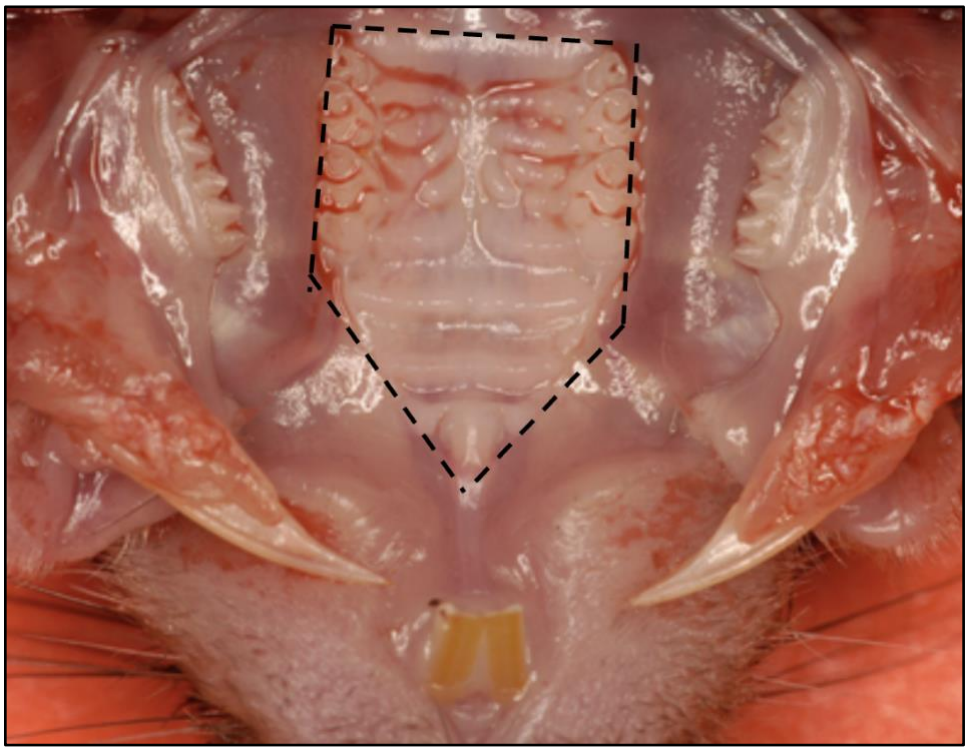

Figure 4: Close View of Nasal Associated Lymphoid Tissue. *This image shows the upper jaw of a rodent to illustrate NALT location. The figure was found in literature but modified with the back dashed lines to indicate the area of the top palette that was excised for the extraction of NALT ((Bittner-Eddy, 2017).*

Mucous membranes are induction sites for immune responses to antigenic material (Debertin, 2003). The nasal cavity area is an attractive spot for vaccine-based mucosal analysis because of its highly vascularized epithelial layer (Kang, 2013). This allows for easier recruitment of circulating immune cells. Intranasal vaccination has shown efficacy, and the application of immunostimulants in vaccines has been shown to help with vaccine efficiency (Debertin, 2003) (Kang, 2013). Under analysis in this study is the nasal-associated lymphoid tissue (NALT), a key structure in the nasal immune system characterized by the aggregation of organized lymphoid tissue (Debertin, 2003). It is located in the upper palette, as seen in **Figure 4**. This tissue is often ideal in the assessment of immune reaction to pathogens as it is the main mucosal inductive site in natural local defense and in vaccination (Kang, 2013).

Intranasal vaccination is an attractive option for treatment method against various pathogens. Because mucous membranes here are a frontline defense, and because of the high immune trafficking in the area, intranasal vaccination is able to assist in both innate and adaptive immunity (Zaman, 2012). In fact, in recent studies, intranasal vaccination has been shown to produce systemic, memory immunity, as opposed to more traditional routes of vaccine administration (Nelson, 2021). Because of this and because the NALT is a high immune reaction site against invading pathogens, combined analysis is an attractive option for detailed immune exploration. The intranasal vaccination method may provide a more universal and versatile treatment option for more common maladies. Furthermore, GC's induced immune activity makes it an attractive option for potent and efficient vaccination.

1.6 Study's Analysis Methods

1.6.1 IVIS and Interferon Reporter Mouse

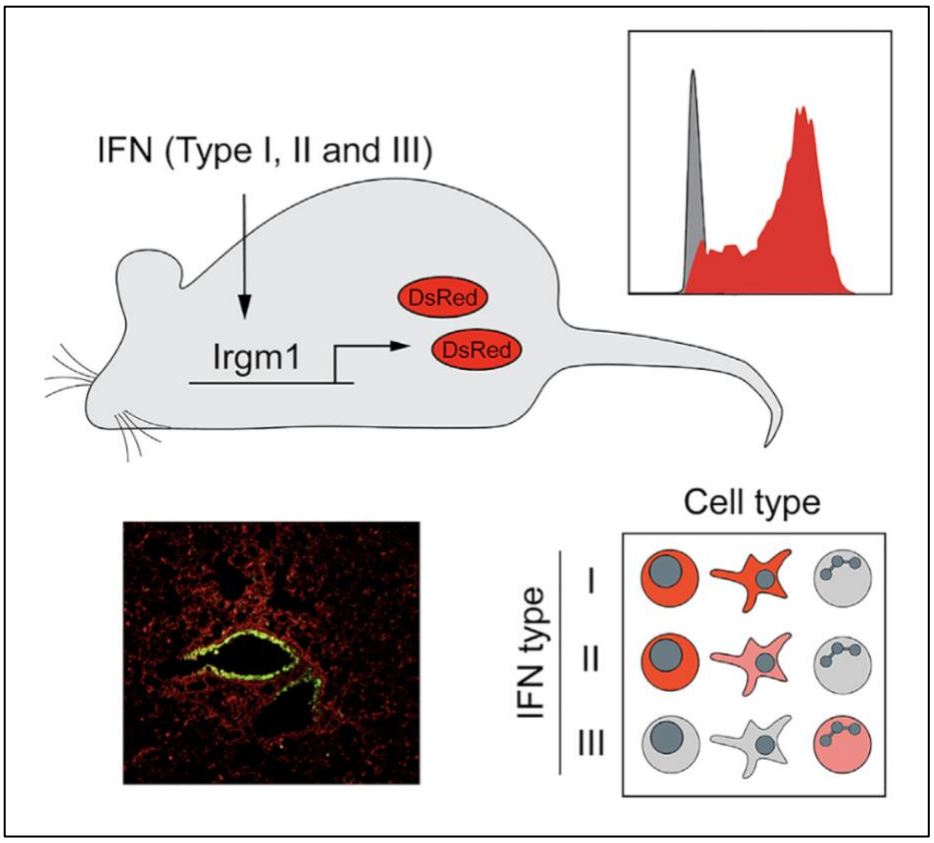

Figure 5: Overview of the function of the interferon reporter mouse. *The top left schematic shows the gene that was modified (Irgm1) to produce the interferon stimulation fluorescence (DsRed). The bottom left schematic is an example of* in vitro *fluorescent imaging to show the activity. These mice can be utilized at different imaging options to report on all types of interferons, but the purposes of this study report on type I. This image is pulled from a literature article that introduced this new strain of mouse and its function((Stifter, 2019).*

Caliper Life Sciences IVIS (In Vivo Imaging System) Spectrum CT is an in vivo imaging modality meant for molecular and anatomical imaging of primarily bioluminescent or fluorescent signals. It is favored for its ability to non-invasively monitor certain cell signaling, gene expression changes, and disease progression (UT Southwestern Medical Center, 2022). The mice used in the imaging sections of this study (Chapter 2) are a new strain of IFN reporter mice

(Jackson Laboratory, 2024). Developed by Jackson Laboratories, these mice put off fluorescence signal in response to interferon stimulation, making them ideal for the response qualification desired in this study (**Figure 5**). They visualize interferon signaling rather than interferon expression, making them ideal for time-series studies in the measurement of continuous immune responses (Stifter, 2019). The IVIS is an ideal tool in quickly and efficiently analyzing this fluorescent response *in vivo* (Cool, 2013).

1.6.2 Bulk-RNA

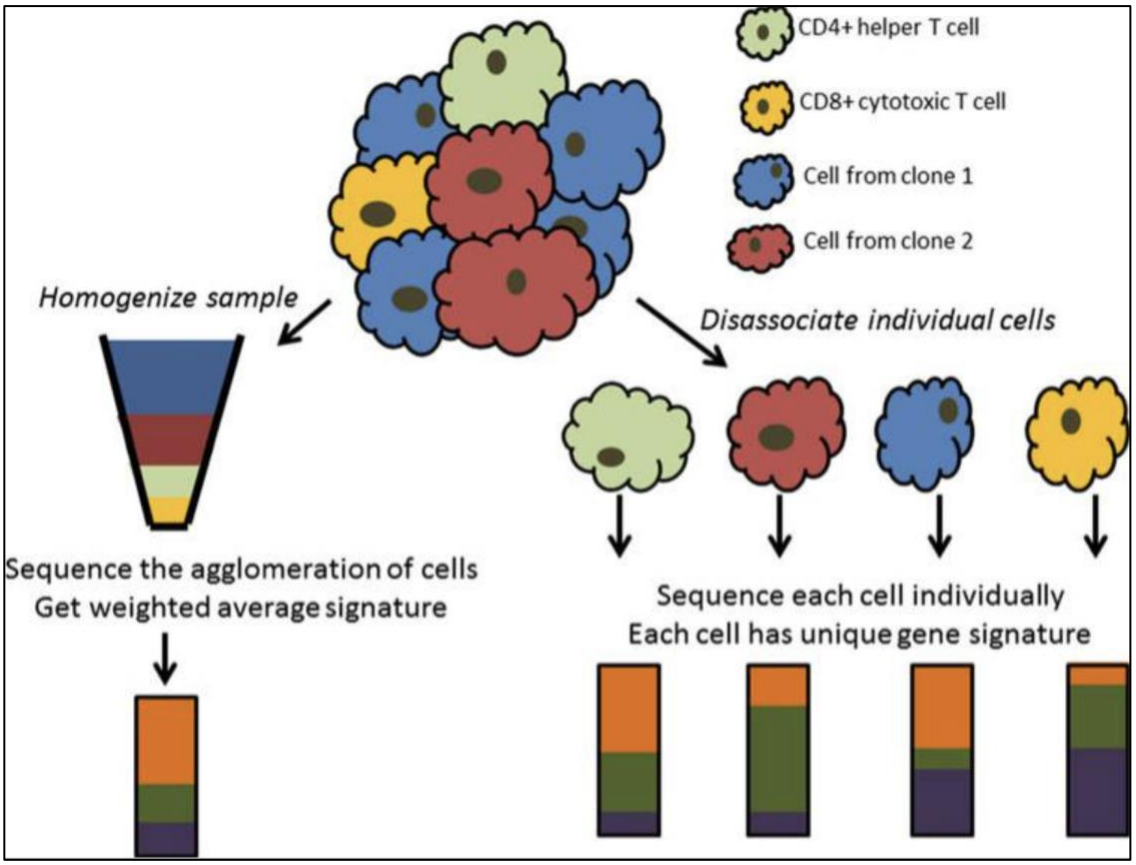

Figure 6: Illustration of differences between bulk-RNA sequencing and single cell RNA sequencing. *This figure was pulled from a literature piece to provide further explanation of the principle of bulk-RNA sequencing ((Yu X. e., 2021). The figure shows the average expression found in bulk sequencing versus the individualized, cell-specific expression found in single cell sequencing.*

Bulk RNA sequencing is the analysis of the total RNA in a population that evaluates the entire transcriptome (Illumina, 2024). Isolated RNA from a sample is converted into cDNA then sequenced to create a library for comparison to a reference genome (Wang, 2009). It measures average gene expression across all cells but does not explore cell-to-cell differences; this is within the realm of single-cell sequencing, as seen in **Figure 6** (CD Genomics, 2024). Bulk sequencing can therefore miss some differences between individual cells, whereas single cell sequencing can capture heterogeneity (Hegenbarth, 2022). Because the NALT is characterized by immune activity, and many immune cells are part of the GC response, determining whether average GC-induced response shows the expected outcome (as per the lab's previous findings) is the approach for this study.

1.7 Objectives

While GC has shown clinical efficacy, its mechanisms are largely unexplored. Previous studies in this lab have shown interferon expression and differential gene expression after GC stimulation in primarily *in vitro* applications. The purpose of the current work was therefore to build upon previous, foundational work in an attempt to prove the hypotheses of GC-initiated immune mechanisms in *in vivo* applications, with particular emphasis on the nasal cavity for expansion of the use of GC beyond cancer therapies. Interferon stimulation assessment and differential gene expression analysis following GC administration will provide further understanding of the mechanism in which GC stimulates antitumor and antiviral immune responses.

Chapter 2

GC Administration Induces a Potent Type-1 IFN Response In Vivo

2.1 Objective

The purpose of this experiment was to use a reporter mouse strain and IVIS imaging technology to prove the interferon response to GC *in vivo* that has been previously hypothesized by this lab.

2.2 Materials

Aqueous solution of N-dihydrogalactochitosan (10mg/mL), also referred to as glycated chitosan (GC), was provided by ImmunoPhotonics, Inc. Male C57BL/6-Tg(Irgm1-DsRed2)1Nci/Mmjax mice (commonly labelled M1Red mice) and female C57BL/6J mice were purchased from Jackson Laboratories; these were bred, and a colony of transgene carriers was developed (Jackson Laboratory). Bio-Serv chlorophyll-free rodent diet was used (Fisher Scientific, CAT#14726615), starting 14 days before the IVIS studies.

2.3 Methods

2.3.1. Intranasal vaccination

1% GC and PBS were combined in a 3:1 ratio, respectively. Due to GC's viscosity, this dilution was performed to allow acquisition into the nasal cavity.

Mice were anesthetized using an isoflurane chamber. Once asleep, mice were transferred to an isoflurane-pumped nasal cone on top of an electric heating pad, to maintain body temperature while under anesthesia. Using a fine-tip Q-Tip, Nair was applied to the strip along the nasal canal, from the tip of the nose to the area between the eyes. The Q-Tip was twisted to ensure that the Nair reached the roots of the hair. It was left on for less than 60 seconds, a PBS-doused cloth piece was used to wipe off the hair, and a different cloth piece was used to clean the area, being sure to remove all traces of the Nair. (Nair was applied the day before injections because in the time immediately following manual hair extraction, the mice will further groom the area – i.e., on the following day, there is a much cleaner bald spot, which is better for imaging constancy.)

The following day, mice were again anesthetized using an isoflurane chamber; once asleep, they were put on their backs. A drop at a time, 10 µL of the GC/PBS mixture was added to each nostril by holding the pipette tip directly above the nostril but not touching. Mice were left on their backs under anesthesia for 5 minutes after application, or until the solution had been fully taken in–marked when the sound of uptake is no longer heard along with the mice's breaths and when none is seen on the outside of the nostril. (It is important to allow complete uptake under anesthesia so that the mice do not sneeze out the solution; it is important to keep them on their backs for gravity's help in solution uptake. See **Figure 26** in Appendix C: IVIS Optimization)

2.3.2. Subcutaneous vaccination

Mice were anesthetized using an isoflurane chamber. Once asleep, mice were put on an isoflurane-pumped nose cone on top of an electric heating pad to maintain body temperature while under anesthesia. Mice were shaved then Nair applied using a fine-tip Q-Tip, rubbed in to

ensure that it reached the roots, to remove all hair around the site for vaccination. It was left on for less than 60 seconds, a PBS-doused cloth piece was used to wipe off the hair, and a different cloth piece was used to clean the area, being sure to remove all traces of the Nair. (Nair was applied the day before injections, with an ointment following, to prevent breakage of the skin during injection.)

The following day, mice were again anesthetized and put on the nasal cone. 100µL of 1% GC was administered subcutaneously to the back flank. Skin was lifted to create a "tent", the syringe needle was inserted, and the solution expelled (the formation of a bubble should be felt under the skin). 100µL was chosen based on previously run optimization protocols for GC in the lab; 100µL is a common injection volume in LIT treatments.

2.3.3. IVIS imaging

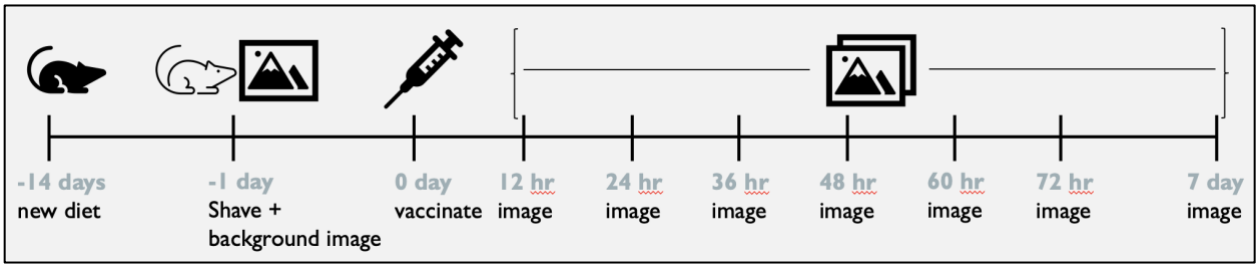

Figure 7: Timeline for IVIS imaging experiment. *This figure shows the various events performed for the IVIS imaging experiment plotted on a timeline (not a continuous interval width). Shown are the diet switch, shaving, vaccination, and various imaging points.*

Two weeks prior to the first imaging time point, mice were switched from the regular rodent chow diet to a chlorophyl-free diet; it takes up to two weeks for the regular chow to make its way out of the mouse's system. Imaging was done at the following time points: background (immediately before vaccination), 12hr, 24hr, 36hr, 48hr, 60hr, 72hr, and 7 day, as seen in **Figure 7**. The DsRed wavelength was measured, as in accordance with the reporter mouse used,

and automatic IVIS imaging settings (for exposure, binning, etc.) were used with epi-illumination fluorescence readings.

2.3.4 Analysis

Same-size ROIs (region of interest) were applied across all groups, with separate ROI regions for each of the subcutaneous and intranasal areas. Radiant efficiency values were computed using the Living Image Software for IVIS Spectrum CT. These raw values were transferred to Excel, where they were processed. Normalization, graphs, and significance were generated using GraphPad Prism.

2.4 Results

2.4.1 IVIS Sequences and ROI Placement

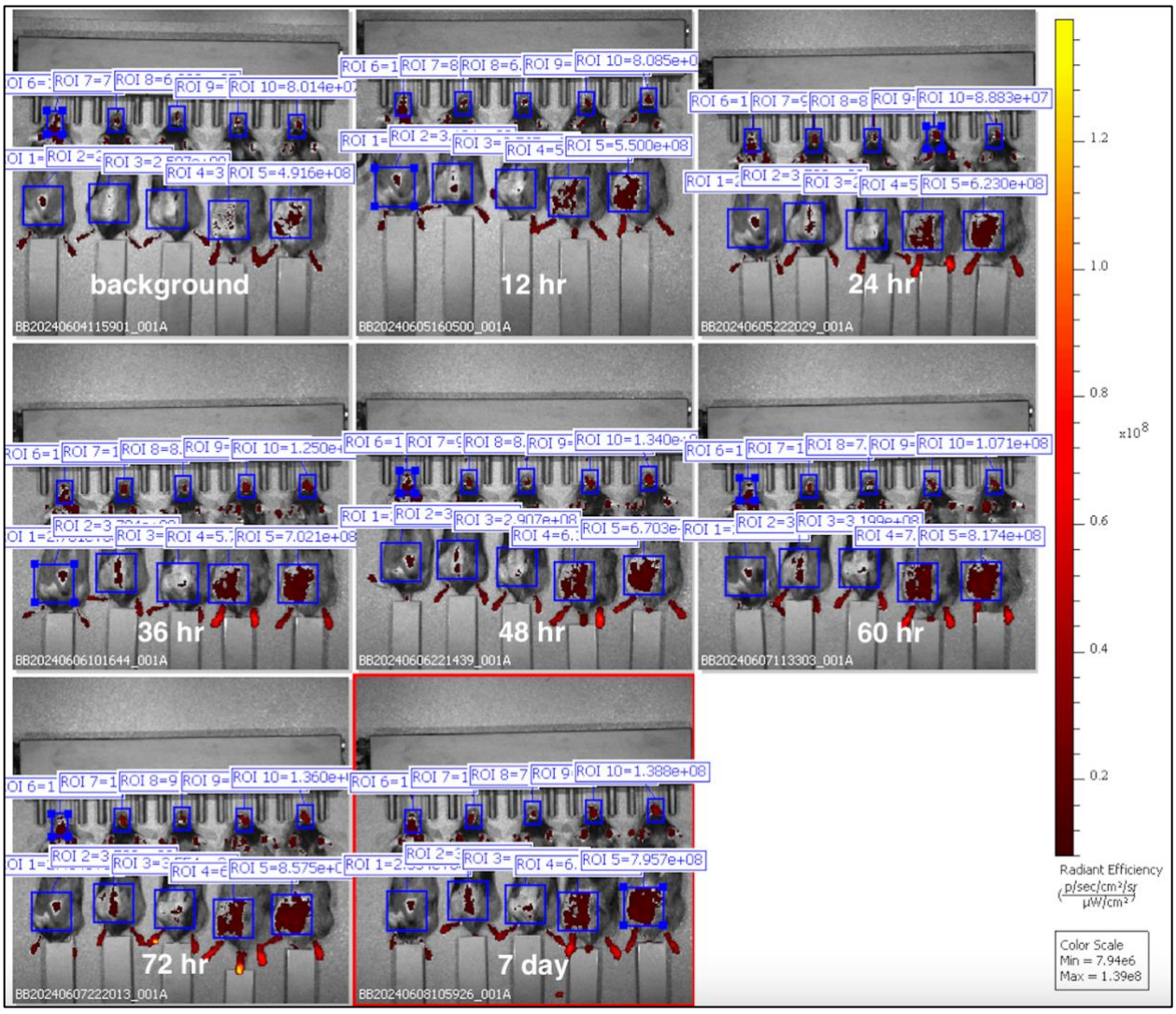

Figure 8: Representation of ROI placement for the IVIS imaging study. *This figure shows the placement of the intranasal and subcutaneous ROI boxes for measurement of total radiant efficiency after GC administration. Two ROIs are placed on each mouse, one in the intranasal area and one in the local subcutaneous area on the hind flank. The group represented here were mice in the control group (i.e., reporter mice with no stimulation). All relevant time points, as mentioned in the methods section, are labelled accordingly.*

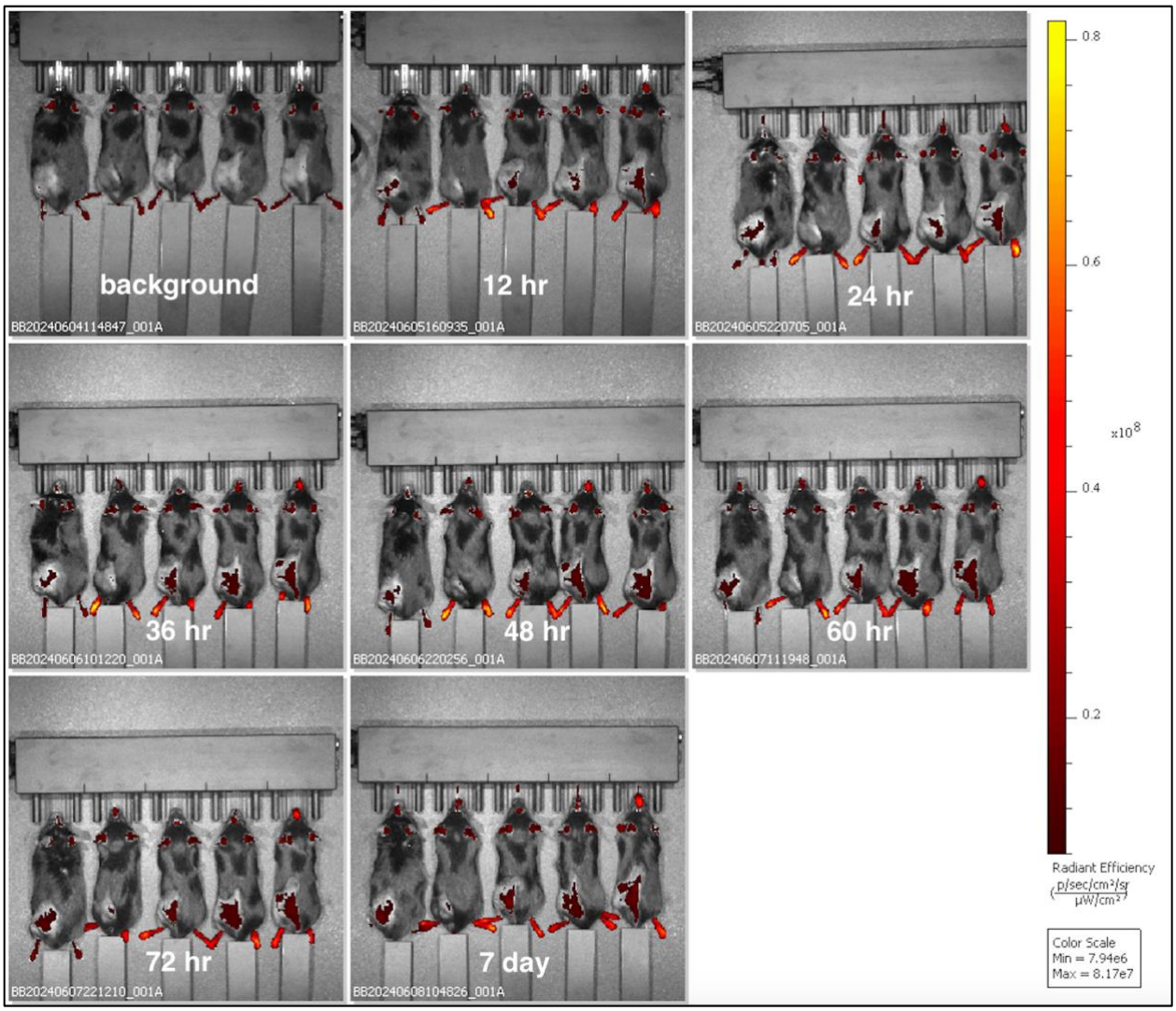

Figure 9: IVIS acquisition images of the 100µL test group for the imaging experiment. *This figure shows the total radiant efficiency reading increases of the intranasal and subcutaneous areas after GC administration. Two areas of fluorescent increase are relevant on each mouse, one in the intranasal area and one in the local subcutaneous area on the hind flank. The group represented here were mice in the 100µL test group. All relevant time points, as mentioned in the methods section, are labelled accordingly.*

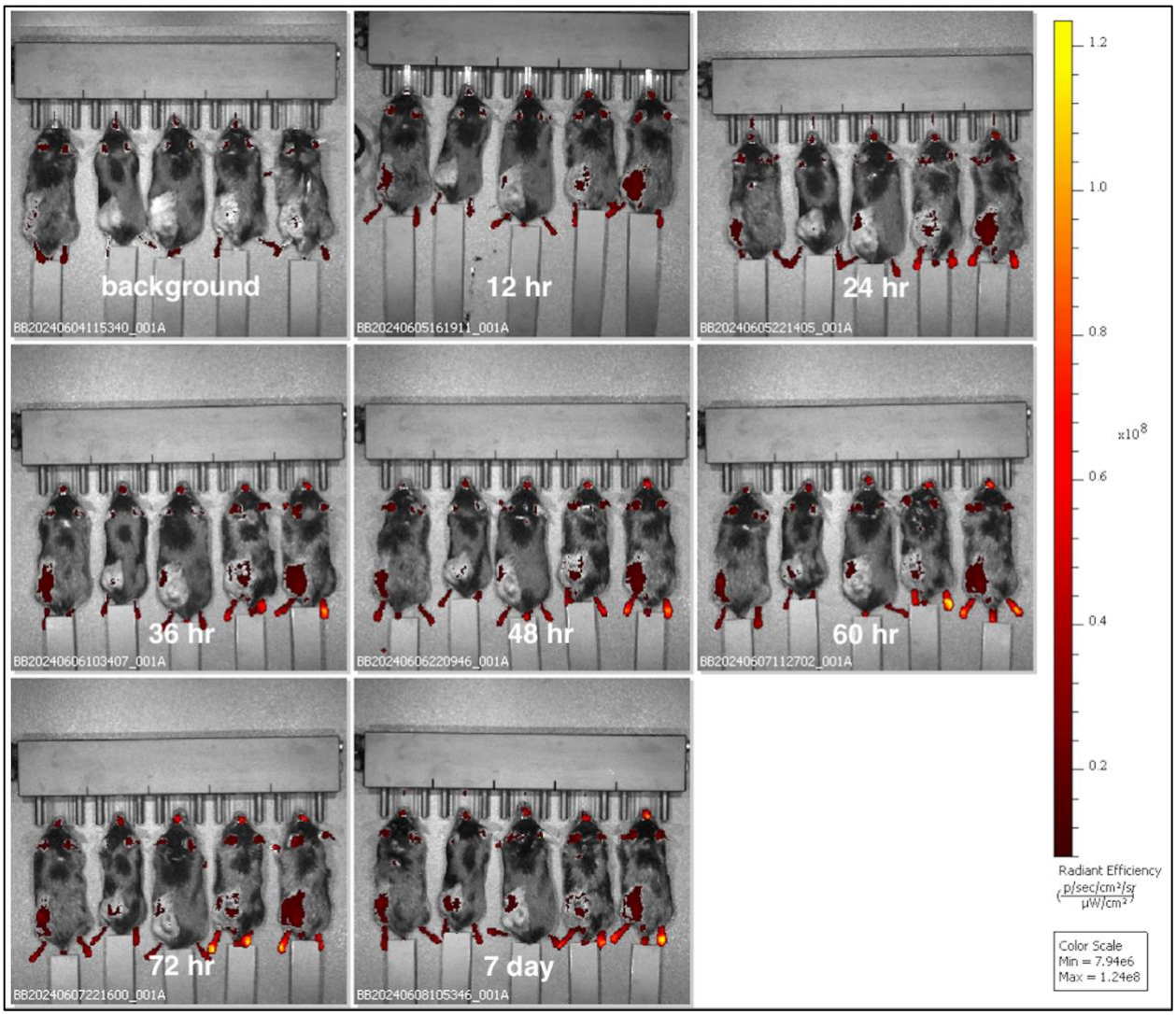

Figure 10: IVIS acquisition images of the 50µL test group for the imaging experiment. *This figure shows the total radiant efficiency reading increases of the intranasal and subcutaneous areas after GC administration. Two areas of fluorescent increase are relevant on each mouse, one in the intranasal area and one in the local subcutaneous area on the hind flank. The group represented here were mice in the 100µL test group. All relevant time points, as mentioned in the methods section, are labelled accordingly.*

Figure 8 shows the IVIS acquisition images of mice in the control group as well as how the placement of the ROIs for total radiant efficiency data acquisition. The two mice on the right of the row of 5 were injured with fight wounds from cage infighting during the course of the study. They were not injured enough to prevent image acquisition, so they were still included to

represent the response of naturally inflicted wounds. **Figure 9** shows the IVIS acquisition images of mice in the 100µL subcutaneous injection test group. **Figure 10** shows the IVIS acquisition images of mice in the 50µL subcutaneous injection test group. In the latter two figures, the potency of the intranasal fluorescence increase is much more clearly visible than is the subcutaneous, as will be later discussed. (ROI areas are not included on the latter two figures so that the actual area of signal can be more clearly seen; the area studied in the first figure applies throughout all test groups).

2.4.2 Intranasal vaccination

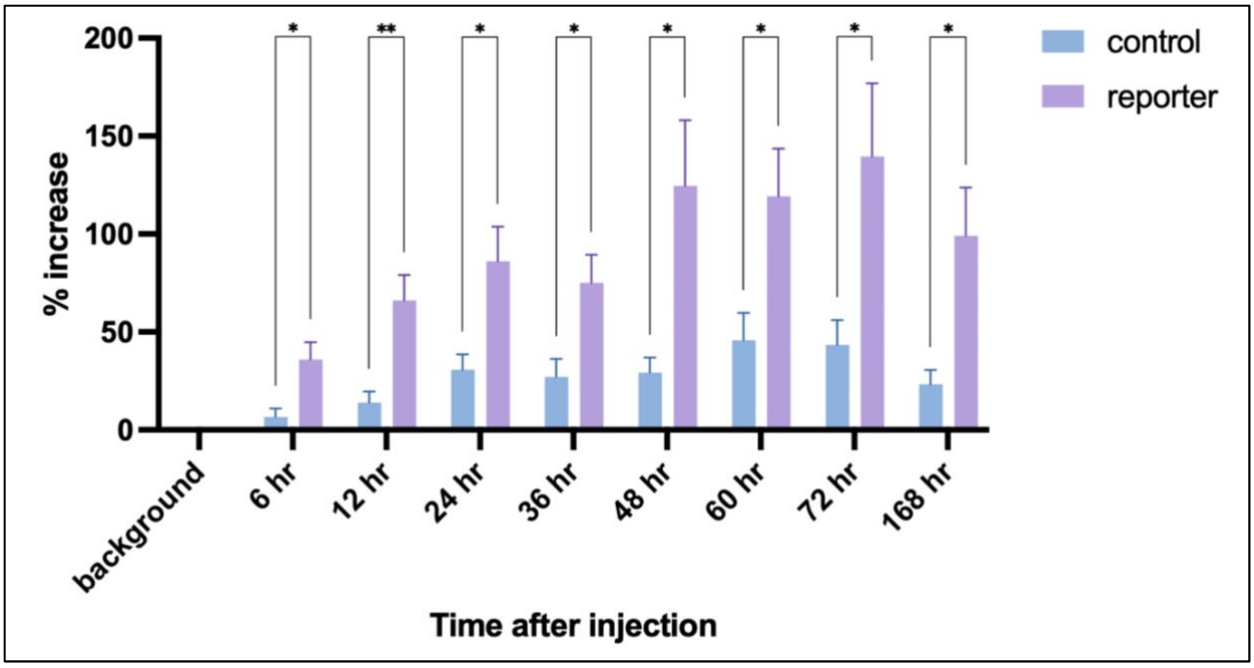

Figure 11: Increase in total radiant efficiency in nasal cavity above background reading after GC administration: control vs test. *Grouped column bar graph depicting the percent increase of total radiant efficiency in the nasal area following intranasal vaccinations, as normalized to the background signal (the imaging time point prior to the vaccination) for each individual treatment group, calculated at time points up to 7 days post-injection. The reporter group indicates the GC-vaccinated interferon reporter mice, whereas the control group indicates the PBS-vaccinated. Significance is calculated for the difference between the control and test group for each time point, for which one star indicates significance greater than 0.05 and two stars indicates greater than 0.01. (Significance readings below 0.1 are not shown.)*

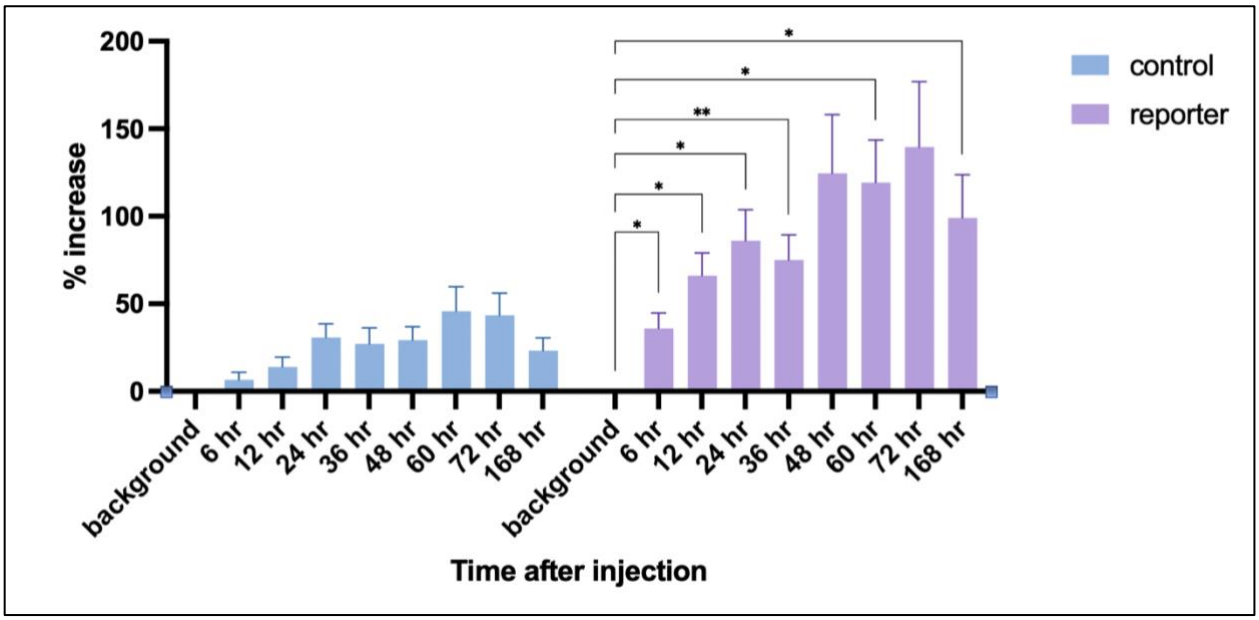

Figure 12: Increase in total radiant efficiency in nasal cavity above background reading after GC administration: time point vs background. *Grouped column bar graph depicting the percent increase of total radiant efficiency in the nasal area following intranasal vaccinations, as normalized to the background signal (the imaging time point prior to the vaccination) for each individual treatment group, calculated at time points up to 7 days post-injection. The reporter group indicates the GC-vaccinated interferon reporter mice, whereas the control group indicates the PBS-vaccinated. Significance is calculated for the difference between the background (i.e., base signal) and each time point for individual test groups, for which one star indicates significance greater than 0.05 and two stars indicates greater than 0.01. (Significance readings below 0.1 are not shown.)*

Figure 11 and **Figure 12** display percentage increase values for total radiant efficiency readings as normalized to the background reading in the nasal cavity, following intranasal GC vaccination. **Figure 11** shows the significant comparisons between the test group and control group at each time point. These have significance at each time point. **Figure 12** shows the significant comparisons between each time point and the background, to show significant increases in readings. These have significance at most test time points and no significance in the control group. (In both, points that do not have comparison significance labelled on the graph do not have high enough statistical significance to be noteworthy (i.e., significance less than 0.1).)

2.4.3 Subcutaneous vaccination

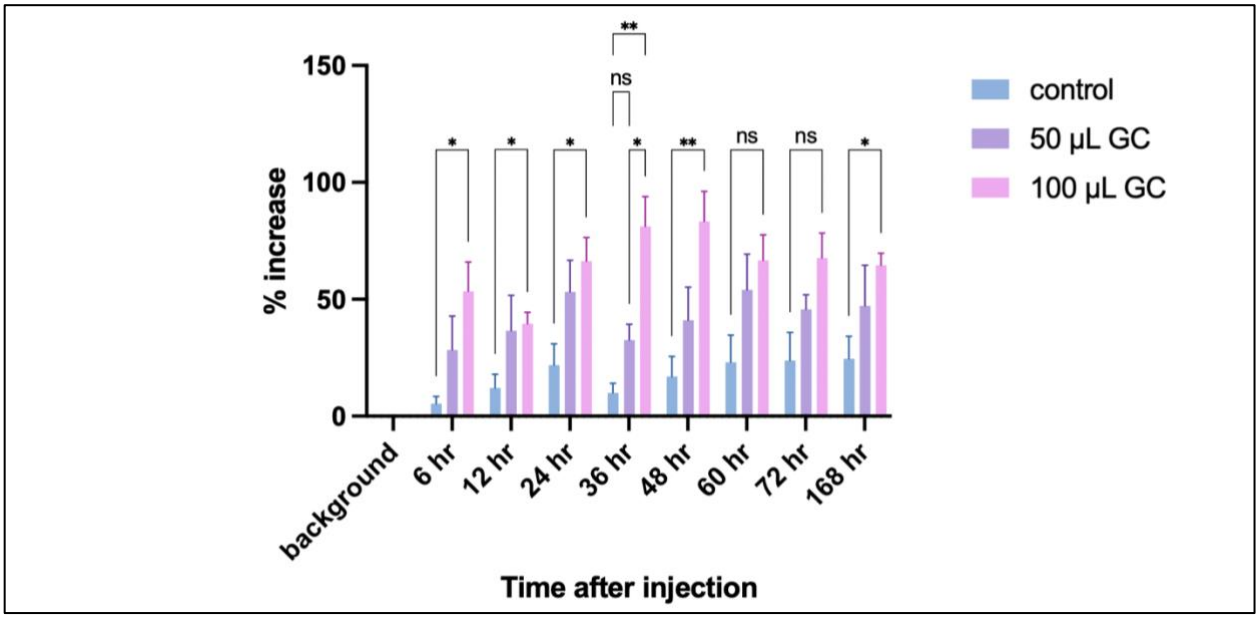

Figure 13: Increase in total radiant efficiency above background reading in area after subcutaneous GC injection: control vs test. *Grouped column bar graph depicting the percent increase of total radiant efficiency in the local area following subcutaneous vaccinations, as normalized to the background signal (the imaging time point prior to the vaccination) for each individual treatment group, calculated at time points up to 7 days post-injection. The reporter group indicates the GC-vaccinated interferon reporter mice, whereas the control group indicates the PBS-vaccinated. Significance is calculated for the difference between the control and test group for each time point, for which one star indicates significance greater than 0.05, two stars indicates greater than 0.01, and "ns" indicates significance between 0.1 and 0.05. (Significance readings below 0.1 are not shown.)*

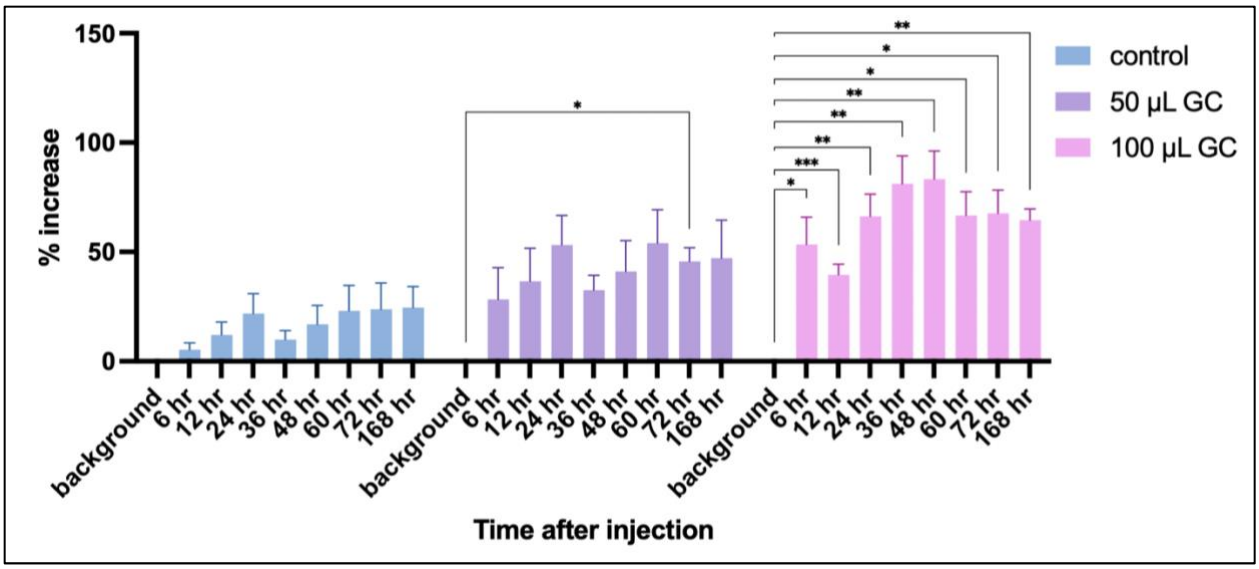

Figure 14: Increase in total radiant efficiency above background reading in area after subcutaneous GC injection: time point vs background. *Grouped column bar graph depicted the percent increase of total radiant efficiency in the local area following subcutaneous vaccinations, as normalized to the background signal (the imaging time point prior to the vaccination) for each individual treatment group, calculated at time points up to 7 days post-injection. The reporter group indicates the GC-vaccinated interferon reporter mice, whereas the control group indicates the PBS-vaccinated. Significance is calculated for the difference between the background (i.e., base signal) and each time point for individual test groups, for which one star indicates significance greater than 0.05, two stars as greater than 0.01, and three stars as greater than 0.001. (Significance readings below 0.1 are not shown.)*

Figure 13 and **Figure 14** display percentage increase values for total radiance efficiency readings as normalized to the background reading in the local area, following subcutaneous GC vaccination. **Figure 13** shows the significant comparisons between the test group and control group at each time point. These have significance at most time points for the 100µL test group and no notable significance for the 50µL group or control group. **Figure 14** shows the significant comparisons between each time point and the background, to show significant increases in readings. These have significance at all test time points for the 100µL group, no consistent significance in the 50µL group, and no significance in the control group. (In both, points that do

not have comparison significance labelled on the graph do not have high enough statistical significance to be noteworthy (i.e., significance less than 0.1).)

In **Figure 11**-**Figure 14**, total radiant efficiency measurements for each time point on each sample were individually normalized to the background, with each time point then being represented as a percentage increase over the background signal, as calculated for each individual sample then averaged. Results are therefore normalized to the baseline fluorescent signal for each mouse, thus showing effective increase in signal. Mice being used are interferon reporter mice, which fluoresce on the DsRed wavelength in response to interferon stimulation. These normalized increases thus represent increase from the interferon signal propagation.

2.5 Discussion

2.5.1 Intranasal application

Figure 11 verifies the change by marking significance between the test group and the control group for each time point. **Figure 12** verifies the change by marking the significance between the background and each time point, for individual test groups. In this way, significant changes are seen as compared to both the control group and the test group's own signal. In **Figure 11**, which shows intranasal fluorescence analysis, every time point tested shows a statistically significant increase of the GC treated group as compared to the untreated for the same time. **Figure 12**, which also shows intranasal fluorescence analysis, almost every time point of the GC group shows a statistically significant increase as compared to the background. Those time points that did not have calculated significance likely lacked it because of the higher standard deviation. Because fluorescence is so variable, smaller test groups (in this case, a group of 10) can outweigh the average change (see **Figure 27** in Appendix C: IVIS Optimization).

While the control group saw some fluctuation, none of it was calculated to be significant, so this change can likely be attributed to normal fluctuation.

2.5.2 Subcutaneous application

Figure 13 verifies the change by marking significance between the test group and the control group for each time point. **Figure 14** verifies the change by marking the significance between the background and each time point, for individual test groups. In this way, we see significant changes as compared to both the control group and the test group's own signal.

In **Figure 13**, which shows subcutaneous fluorescence interpretations, every time point tested shows some measure of statistical significance between the untreated and the 100µL GC treated. The 60h and 72h points show less than the desired significance, but still a respectable level. The difference in these two versus in the others is likely in the smaller test group. In between the 48h and 60h time points, one of the mouse cages being used saw extreme in-fighting, causing wounds in a few of the mice too great for them to continue in the study. Would that these mice had continued the study, we would likely see the same level of significance as priorly.

Figure 14 shows that every single time point showed a significant increase as compared to the background, whereas the other groups mostly did not. However, as seen in **Figure 13**, not every single increase was as statistically significant as compared to the control's percent increase. The 50µL GC injection was also tested to see whether a smaller dosage in vivo could still elicit a potent response. As seen in **Figure 13** and **Figure 14**, while the 50µL group did show an increase, it was not statistically significant. However, the error bars in this group show to be slightly larger, on average, so this may hinder shown results (as previously discussed with

the relatively small test group sizes). Regardless of these minor dips in significance, this work still shows promising preliminary results in interferon activation to lead into a larger study.

It should be noted here, as a comparison, that the intranasal results produced equally significant results as the 5X larger volume. This holds significance in terms of application of this immunoadjuvant in future treatment application. Not only does it save resources with a smaller volume able to produce the same response, but it also supports the extension of GC into intranasal vaccination treatment practice. This is significant findings because, as mentioned previously, intranasal administration holds great promise in improved treatment efficacy and immune memory generation.

2.5.3 IVIS Field of View

For the purposes of this study, because there were two localized spots on opposite sides of the body being imaged and because so many mice were being done at a time (relatively, in terms of the time for acquisition on the IVIS machine), IVIS field of view (FOV) D was used (see Appendix C: IVIS Optimization for a visualization of the view differences). In this view, 5 mice may be imaged at once. In consideration of the time for acquisition: 4 minutes to anesthetize the mouse and 6 minutes for the two separate acquisitions. At 10 minutes per mouse, the time difference from the first to the last mouse could cause significant differences in terms of immune response timeline. Additionally, because of the nature of this study in terms of time points, the length of experiment running at times outside of normal operating hours, as previously discussed, could have caused more detriment in disruption of mouse rhythms. However, now that this preliminary data has been set, time points could be adjusted to be fewer and within regular hours; this obstacle could be circumvented. Performing this study at the

farther FOV may generate less accurate or less tissue-penetrating readings as compared to a closer view (e.g., FOV A), but it nonetheless produced significant results in this study.

2.5.4 Adverse reactions

In the 100µL injection group, most mice experienced an adverse reaction of necrosis around the site of injection (see Appendix A: IVIS Adverse Reactions). In addition to this necrosis, the "bubble" of injection under the skin turned hard and stayed for over 14 days post-injection. Necrosis did not occur in the 50 µL injection group, but the mass at injection site only persisted for 7 days. Further experimentation may help narrow down to the cause of this problem.

This injection volume has been used in other studies in the lab many times and has not caused this reaction before. Some hypothesized reasons for this are as follows. First, GC is a very viscous fluid, so it may need to be diluted more to allow it to dissipate from the injection site. Because the same reaction did not occur in the 50µL injection group, this cause only applies for higher volumes. Secondly, it is possible that because the GC was administered alone (i.e., there was no existing response to amplify), the response generated may have turned inwardly attacking and caused a build-up under the skin. If this were the case, or possibly a combination of the two, the effect could possibly be mitigated by finding a volume that does not cause necrosis but still produces a notable response. However, some of the wounds looked as if they could have been self-inflicted or inflicted by cage mates. That type of reaction to a skin disturbance has been previously in the lab as well. It is possible that the large volume at the given viscosity caused the mouse enough irritation for it to bite or scratch the area. The resulting wound combined with the heightened immune environment could have caused the negative effect.

2.5.4 Potential Limitations

Fluorescent signal *in vivo* in mice fluctuates often depending on anything from diet to hair length to time of day. Even with the mice on a chlorophyl-free diet to reduce noise (see Appendix C: IVIS Optimization), there is still fluctuation, as evidenced by the changes seen in the control group, which should have had no direct immune stimulation. Part of the fluctuation in this study specifically may also be attributed to the fact that the mice had to be used outside of the typical window of operating hours; this interferes with their natural circadian rhythm and therefore may have caused slight changes due to stress (Hylander, 2022). In addition to the abnormal experimental hours is the high number of run times in such a short period of time. The mice underwent many rounds of anesthesia, which may have further impacted their resting state due to added stress. Thus, the need for normalization to a base signal was necessary to determine effective validity of results. Despite these potential limitations of fluorescence, the intranasal and subcutaneous GC vaccinations still produced a potent type I interferon response *in vivo*.

Chapter 3

Differential Gene Expression After GC Administration

3.1 Objective

The purpose of this experiment was to qualify the interferon response results found in the IVIS experiment discussed in Chapter 2. While the IVIS experiment showed that there was in fact in a response of quantitative significance, this experiment aimed to further elucidate the specific mechanisms by which that response was achieved.

3.2. Materials

Aqueous solution of N-dihydrogalactochitosan, more commonly known as glycated chitosan (GC) (10mg/mL,1%), was provided by ImmunoPhotonics, Inc. Female 8-week-old C57BL/6J mice were purchased from Jackson Laboratories. The Quick-RNA Microprep Kit was purchased from Zymo Research (Cat# R1051). The Omni Ruptor Elite homogenizer was borrowed from the Dr. John Clegg, here at the University of Oklahoma; Hard Tissue Homogenizing Ceramic Bead Filled Tubes were purchased from Omni International. RNAase Away Surface Decontaminant spray was purchased from Thermo Scientific.

3.3. Methods

3.3.1. Intranasal vaccination

1% GC and PBS were combined in a 3:1 ratio, respectively. Due to GC's viscosity, this dilution was performed to allow acquisition into the nasal cavity.

Mice were anesthetized using an isoflurane chamber; once under, they were put on their backs. A drop at a time, 10 µL of the GC/PBS mixture was added to each nostril by holding the pipette tip directly above the nostril but not touching. Mice were left on their backs under anesthesia for 5 minutes after application, or until the solution had been fully taken in–marked when the sound of uptake is no longer heard along with the mice's breaths and none is seen on the outside of the nostril. (It is important to allow complete uptake under anesthesia so that the mice do not sneeze out the solution; it is important to keep them on their backs for gravity's help in solution uptake.) (For picture-based reference and in-depth detailing, (Agostino, 2022) is particularly helpful.)

3.3.2. NALT extraction

Figure 15: Timeline for NALT RNA sequencing experiment. *This figure shows the various events performed for the vaccination and NALT extraction in the RNA sequencing experiment, as plotted on a timeline (not a continuous interval width). Shown are the vaccination and multiple group-based harvesting time points.*

At time points of 24-, 48-, and 72-hours post-GC administration, mice were euthanized and NALT extraction performed. The euthanized mouse was placed on its back, and pins were

used in the four feet and at the tip of the nose to secure the specimen. The jaw was cut open on both sides, removing the lower mandible, and excess blood was washed and wiped away with cold PBS and sterile cloth. A scalpel was run along all sides of the palette on the top mandible to detach it. The tissue piece was then gripped at the top with forceps and gently lifted off by pulling in the opposite direction of the nose, avoiding tearing (scalpel was sometimes further required to cut any tissue connections underneath the palette). The NALT was then washed twice in a well of a plate filled with PBS, swishing around gently to get rid of excess blood, hair, or other contaminating elements. The tissue piece was then transferred to a 2mL bead-beating tube for the homogenization step. (More detailed protocols for this surgery can be found in the literature (JoVE Journal, 2012) (A Nacer, 2014).)

All surgical tools, workspace, and hands were thoroughly cleaned with RNAase Away spray and ethanol in between subjects. Proper PPE, including a mask and hair net to ensure no downfall of DNA contamination from the person to the sample, were worn at all times.

3.3.3. RNA extraction and preparation

The bead-beating tube containing Lysis Buffer and the NALT, was then put through 4 15 second running intervals on medium speed, or until no large tissue pieces were visible within the tube.

RNA preparation from the extracted NALT tissue was performed using the Zymo prep kit and conducted according to the manufacturer's instructions, as given in the manual.

3.3.4. RNA processing and sequencing

For sequencing, RNA preparation and sequencing service were performed by the OUHSC Genomics Lab, with library preparation and sequencing performed on the NextSeq 2000 machine from Illumina. Further explanation of this process can be found in Appendix B.

3.3.5 Previous study's BMDC culture and stimulation

BMDCs underwent a 24-hour stimulation with GC then were harvested and stained (with BV510, CD11b, APC-Cy7, and CD11c FITC). Live cells positive for the markers were then isolated using FACS sorting and put through an RNA isolation protocol using the Zymo kit mentioned in the Materials section. Further information about sequencing and bioinformatics specifics can be found in Appendix B (Hoover, 2022).

3.4. Results

3.4.1 Study basis

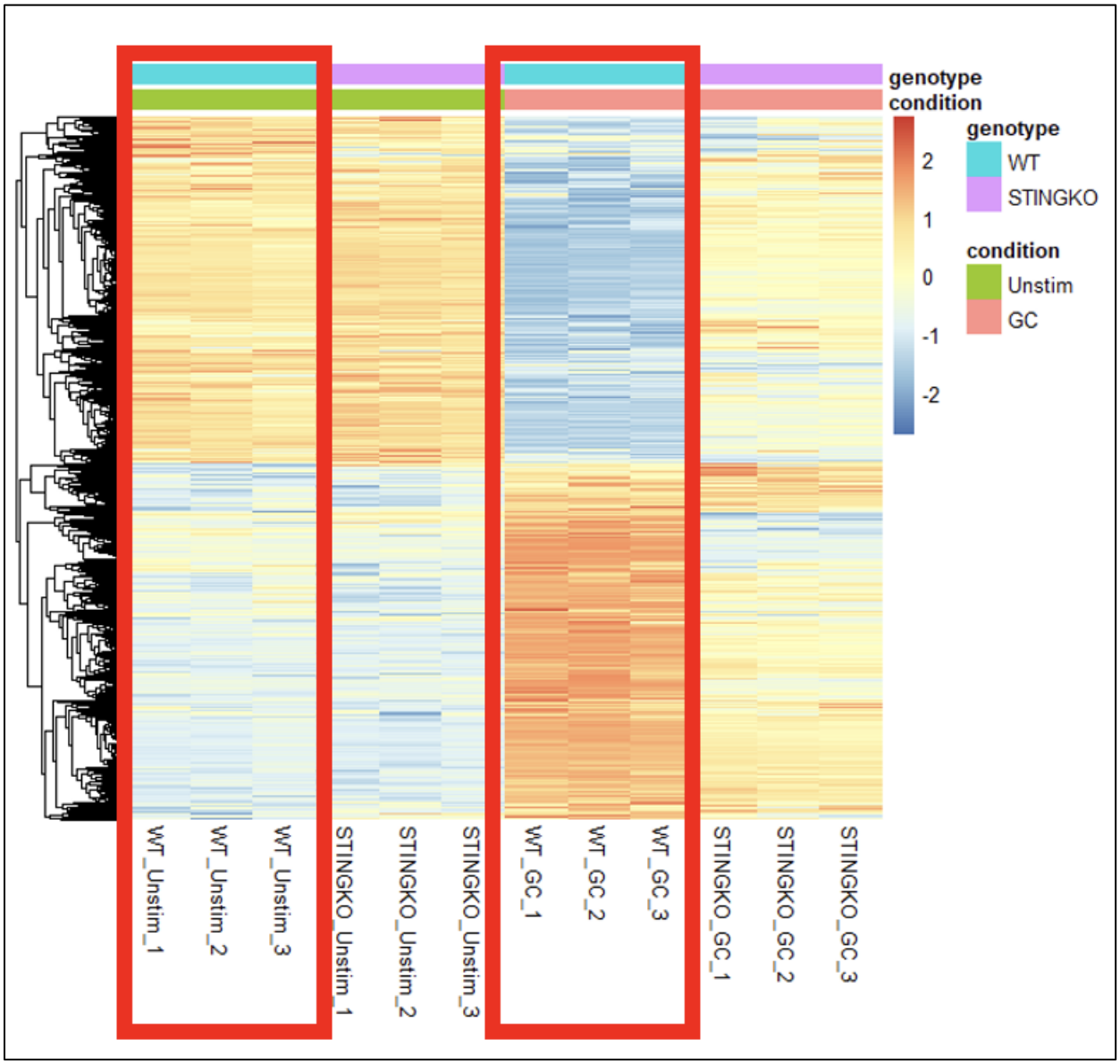

Figure 16: Gene Differential Expression of wild-type BMDCs GC-stimulated vs Unstimulated. *Heatmap illustrating comparisons between treatment groups in gene expression variability counts. Results were generated from RNA sequencing data from BMDCs stimulated for 24 hours before being stained, sorted, and isolated for RNA content. Highlighted is the comparison in wild-type mice between unstimulated and GC treated groups. (These results are from a previously run experiment in the lab, which I am using for reference purposes.) (Hoover, 2022)*

Figure 16 shows a trend of differential gene expression upon GC administration in BMDCs, found in a study performed previously in the lab. The protocol for BMDC treatment can be found in Appendix B: Previous RNA Sequencing. This study was used as the basis and inspiration for the current study's efforts, and as a guideline for what results should show. In the figure, the two boxes indicate the two test groups using wild-type mice BMDC's, one group unstimulated and the other stimulated with GC. It shows a clear difference in gene expression in the BMDCs upon GC stimulation.

3.4.2 Current results versus previous results

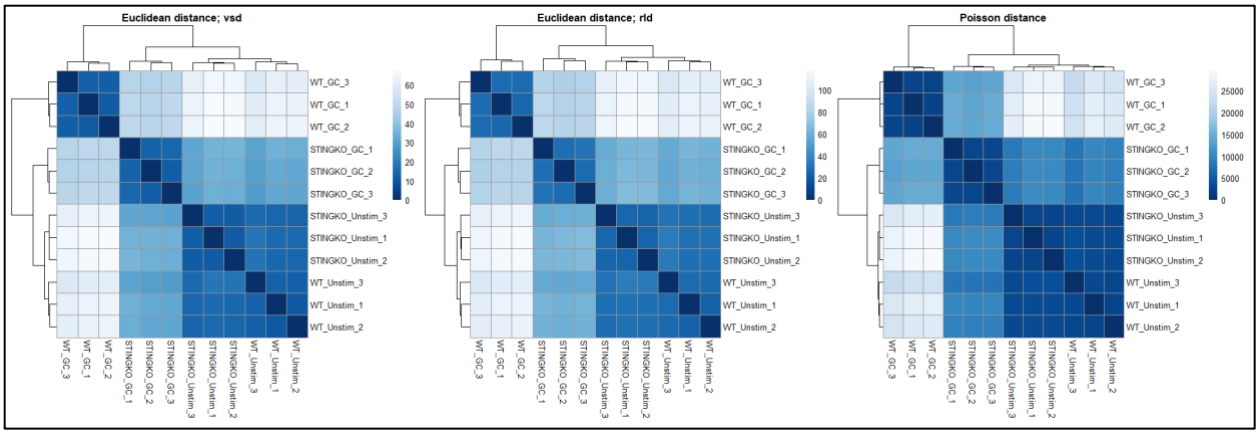

Figure 17: Previous experiment's distance heat map. *Heat maps for distance data of RNA samples generated from RNA sequencing data from BMDCs that were stimulated for 24 hours before being stained, sorted, and isolated. Different test groups are classified under two variables: genotype (STING knockout vs WT) and treatment (unstimulated vs GC stimulated). (These results are from a previously run experiment in the lab, which I am using for comparison purposes. Methods for this can be found in Appendix B.) A higher divergence in expression profiles is indicated by a larger distance. (Hoover, 2022)*

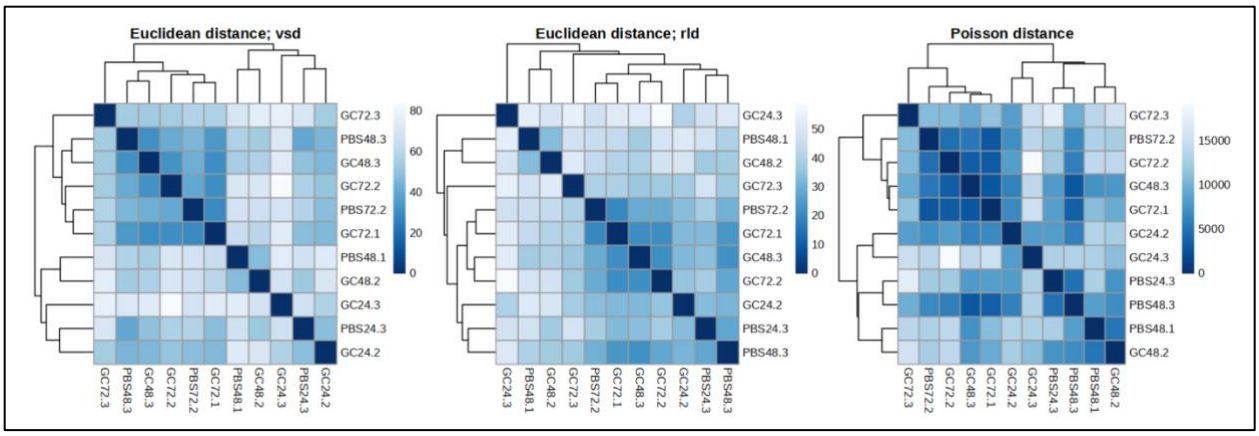

Figure 18: Current experiment's distance heat map. *Heat maps for distance data of RNA samples generated from RNA sequencing data from homogenized NALT following intranasal vaccination. Samples names provide vaccination solution in letters (vaccination with GC or with PBS) then time point post-vaccination of tissue collection in numbers (24h, 48h, or 72h) then sample number (mouse 1, 2, or 3 for the respective group). A higher divergence in expression profiles is indicated by a larger distance.*

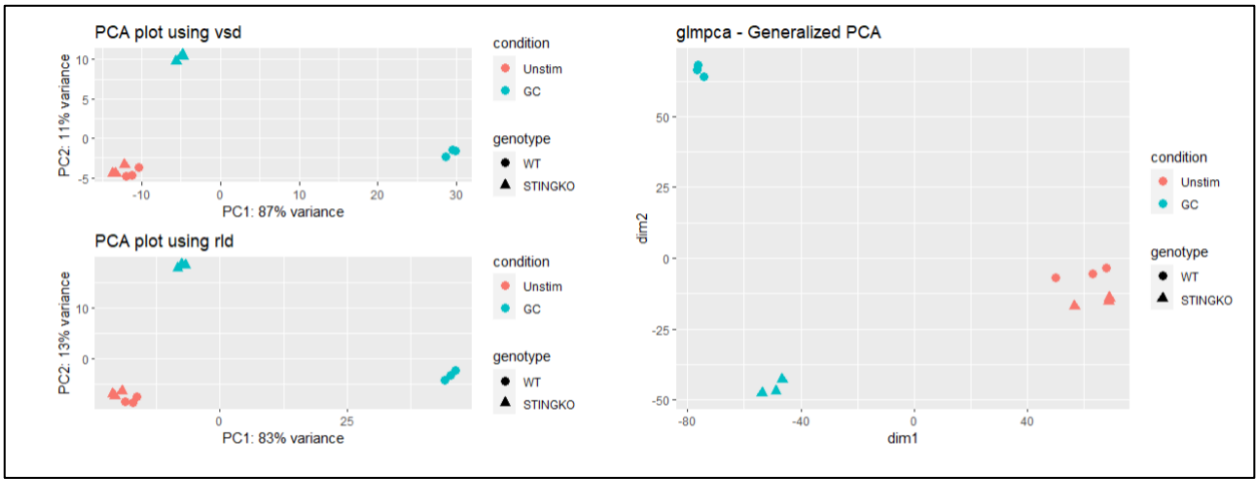

Figure 19: Previous experiment's PCA plots with variance stabilization. *PCA plots of various subsets for the BMDC data, as previously referenced. Graph formulation utilizes count data from RNA sequencing reads from RNA isolated post-GC-stimulation. Samples are divided under two variable types: genotype (STINGKO vs WT) and treatment (GC stimulated vs unstimulated). (Hoover, 2022)*

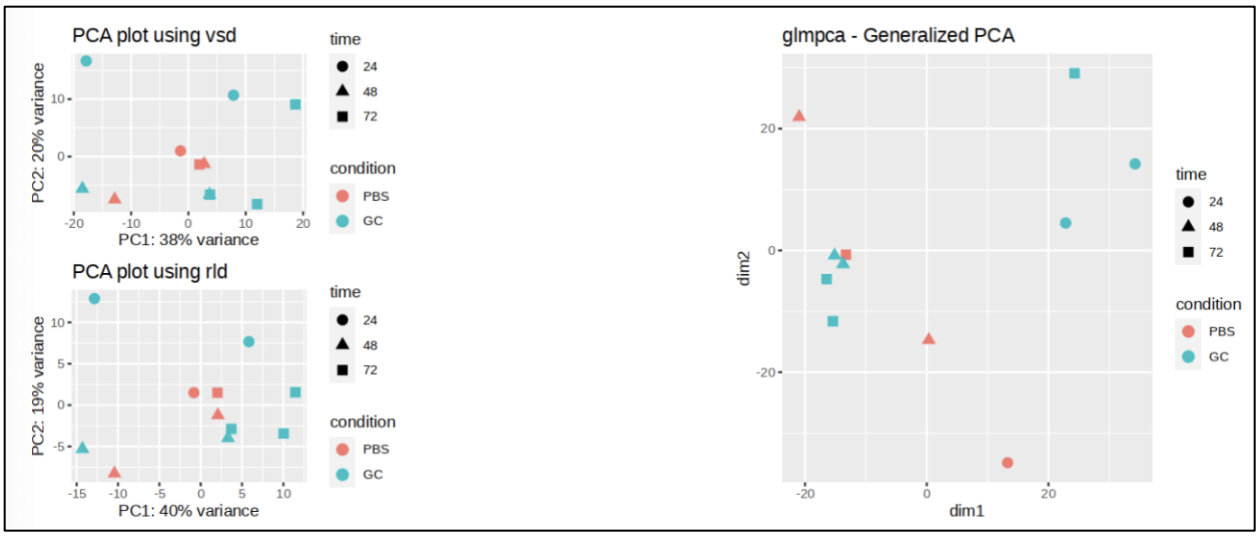

Figure 20: Current experiment's PCA plots with variance stabilization. *PCA plots of various subsets for the NALT data, as completed for this study. Graph formulation utilizes count data from RNA sequencing reads from RNA isolated post-GC intranasal administration. Samples are divided under two variable types: treatment (GC stimulated or PBS stimulated) and time point post-vaccination of tissue harvest (24h, 48h, or 72h).*

Euclidean distance maps depict differential gene expression by illustrating divergence between expression profiles. In these graph types, the larger distance (with color indicated on the scale) correlates to a higher divergence between samples (Mushegian, 2010). Poisson distance maps are also a measure of genetic similarity but are instead generated based on individual gene expression counts. **Figure 17** shows various distance map results from the previous BMDC study and serves as a comparison for what uniform results with distinct differences across test groups should look like. **Figure 18** shows distance map results from this current study and shows no discernible results across test group expression profiles. Samples of the same groups do not relate, and there is no uniform distribution for any of them.

PCA plots, otherwise known as principal component analysis, show similarities and variance considerations between samples in genetic profiling. The two axes are in the two directions that separate the data points the most, with variance for both labelled alongside (Love,

2015). These are, to put it simply, just another depiction of genetic expression profile differences, in another manner than in the distance maps shown before. **Figure 19** shows various PCA plot results from the previous BMDC study and serves as a comparison for what uniform results with distinct differences across test groups should look like. **Figure 20** shows PCA plot results from this current study and shows no discernible results across test group expression profiles. Samples of the same groups do not relate, and there is no uniform distribution for any of them.

3.4.3 Sample RNA readings

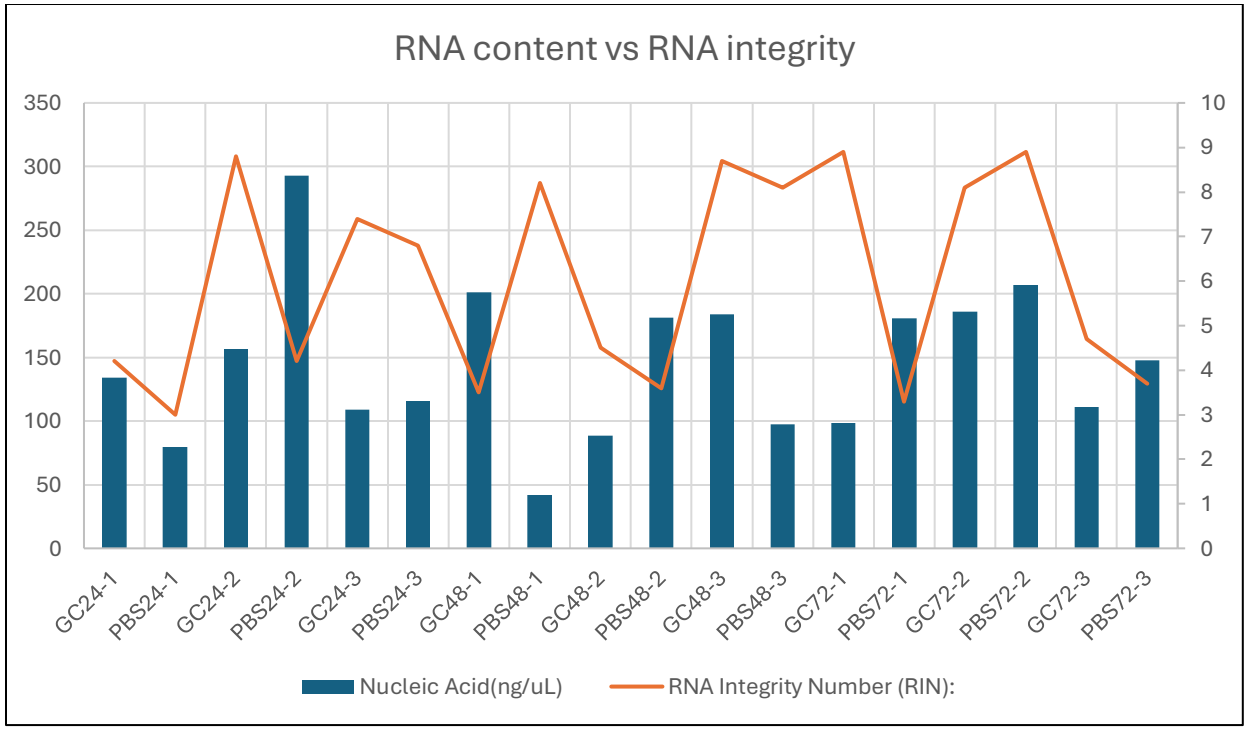

Figure 21: RNA content vs RNA integrity. *Bar graph with secondary axis graph depicting a sample-by-sample comparison of each sample's RNA integrity number (RIN) and nucleic acid content amount (ng/µL), where each sample is the RNA content isolated from extracted murine NALT following intranasal vaccination. Sample names provide vaccination solution in letters (vaccination with GC or with PBS) then time point post- vaccination of tissue collection in umbers (24h, 48h, or 72h) then sample number (mouse 1, 2, or 3 for the respective group). Attempt to show trend or lack thereof between the values for each sample.*

Prior to sequencing, samples submitted for the process undergo a sample quality verification process to ensure that libraries built from the data will be reflective of the true nature of the sample. For example, a low RNA content could corrupt the produced results, and a low RNA integrity number (RIN) could indicate that the full spread of the tissue's RNA content is not reflected. Both of these measures are reflected for each sample in **Figure 21**. An RIN below the threshold of 7 is not recommended for throughput in sequencing. In experimental setup for this procedure, 3 mice per group were used. However, only 11 of 18 samples were put through to the sequencing stage, as they had RINs below the threshold.

3.5 Discussion

3.5.1 Expression difference interpretation

Figure 16 illustrates the clear GC-induced gene expression up-/down-regulation, as proved in the referenced previous study. This study was done *in vitro* in BMDCs, which laid the basis for changing the location to find the initiation location of the immune response from GC.

Figure 17 and **Figure 19** are from the previous study's BMDC RNA sequencing. These graphs show a clear trend of similarities between the different test groups, where the unstimulated groups are nearly identical, and the two stimulated groups show significant differences; these two show the clear expression difference that lend to the proof of STING's participation in the GC mechanism.

Figure 18 and **Figure 20** are from the current study's NALT RNA sequencing. When compared to the BMDC graphs, it is clear that the NALT data had no clear trend in expression differences. There is no clear trend across treatment groups and not even a similar grouping

based on individual treatment types. As seen in the PCA plots of **Figure 20**, there are no similar locations for the time point (shape) or treatment type (color); the plots are all over the map.

3.5.2 RNA quality assessment

Upon receipt from OUHSC of library prep data of RNA samples, it was seen that the sample characteristics were all over the board. Two main indicators of sample quality are the nucleic acid concentration (RNA quantity) and RNA integrity number (RIN). Oddly, there was no trend in group type of the lower quality samples, i.e., the low RIN samples were not all of one treatment type or all of one time point. This leaves the possibilities of corruption source very broad.

Another consideration besides low quality in one treatment group is then whether the two measures of low quality are both low in the samples that were not passed through to the sequencing phase. **Figure 21** shows the attempt at correlation between RNA quality (RIN) and RNA quantity (nucleic acid concentration). As can be seen, there is no similar trend in quality vs quantity per sample. Some of the values that have the lowest nucleic acid concentrations have the highest RINs. This in fact may have lent to the expression profile variability. A low enough amount of RNA content may skew library results, as will RIN (Romero, 2014). Thus, if a sample was used in the reads because it had a high enough RIN but had a very low nucleic acid concentration, the sample may not have been entirely representative of the actual environment (PennState: Huck Institutes of the Life Sciences, 2024). So, even those samples that had high enough RIN numbers to run through sequencing did not produce any sensible results, as seen in **Figure 18** and **Figure 20**. This indicates a problem within the execution, rather than in the experimental design.

3.5.3 Reasons for variable results

All appropriate sanitary and sterilization protocol was followed during surgery and sample handling during all rounds, so corruption seems unlikely. Possible reasons hypothesized for this variability of the NALT experiment results lie in the homogenization method. Because the NALT is a rough tissue, to ensure complete tissue dissociation, more time under homogenization was employed. Immune cells tend to be fragile, as does RNA, so there is possibility that the homogenization method used was too rough and destroyed the desired immune cells. RNA expression changes can be triggered by sample manipulation, i.e., too much time under homogenization run may have contributed to the differential RNA expression levels (Fordyce, 2013). Additionally, because the NALT is a low-yield tissue already, care must be taken to a certain extent to ensure that a workable level of nucleic acid concentration is maintained (Cisney, 2012).

NALT is a front-line of defense for intranasal pathogens, thus making it a popular study point for reactions to pathogens and intranasal vaccines (Shim, 2020). This location should have therefore been appropriate to show the immediate response. As it is typically characterized by heightened immune activity, the complete lack of organized immune activity shown in differential gene expression analysis may again likely be attributed to the homogenization method.

The used method of homogenization was chosen as per the recommendation of the Zymo kit. The bead-beating tube method, as per the manual, is “recommended for complete and efficient homogenization of tough-to-lyse samples”, which should be fit for the NALT tissue. Because the NALT is tough and fibrous as well, many typical homogenization methods may not be fit for complete dissociation and lysis. The need here is a method that is strong enough to

dissociate the tissue but gentle enough to maintain the integrity of the RNA and immune cells. What may be required is simply optimization with the bead-beating method to find this balance. However, one con of the bead-beating machine used is that the process was done with the lysis buffer. Because it is a basic buffer, the mechanical agitation caused foam formation, making it difficult to see whether the contents of the tube included any large tissue pieces; the machine may have therefore been run for more rounds than was necessary. For this reason, another method such as a hand-held tissue homogenizer may be more appropriate so that real time visualization and assessment of dissociation status may be assessed.

Previous studies found in literature mostly utilized a more intense inoculation, so there is a much larger immune response to be capitalized upon. For example, in (Stifter, 2019), influenza was administered to produce a notable response for imaging. In (Shim, 2020), chitosan nanoparticles (chitosan being the immunoadjuvant parent of GC) were loaded with *B. abortus* MdH. Both of these studies allow the initiation of larger-scale immune response than an immunoadjuvant alone. Furthermore, in this lab, cellular imaging studies have been done after treatment with GC + COVID recombinant proteins, in which significant differences in immunohistology were shown. Furthermore, as a more specific relation to this study, in a recent study, interferon genes showed upregulation in NALT cells after COVID-19 infection (Coates, 2023). In the prior study referenced in **Figure 16**, only GC was used, but this stimulation was done *in vitro* rather than *in vivo*, as this current study was, so this may affect the possible scope of reaction. Cellular responses in vitro (in a well plate) are much more controlled than are *in vivo* studies, so the sole immunoadjuvant application has the ability to make more of an impact.

Chapter 4

Conclusions and Future Directions

4.1 Conclusion

The current work showed significant results in the intranasal and subcutaneous localized upregulation of interferon response induced by GC administration, as measured by IVIS Spectrum CT imaging. There were significant differences in total radiant efficiency readings at each time point for the test group compared to the control (intranasally, **Figure 11**, and subcutaneously, **Figure 13**). There were also significant differences seen for the main test group compared to its background signal (intranasally, **Figure 12**, and subcutaneously, **Figure 14**). This activity has been hypothesized and preliminarily proven in certain models previously in the lab. This current work provides proof of and quantification of the activity in the intranasal and subcutaneous areas and lays the groundwork for further studies to determine mechanism. (This study also explored both a strain of mice and a method of imaging new to this lab, which breaks ground and holds promise for future experiments in the lab as well.)

The previous study, via bulk-RNA sequencing, showed that there is a difference in expression of immune-associated genes following GC administration in BMDCs, as seen in **Figure 16**. The current study aimed to find similar up-/downregulation in the nasal cavity to provide basis for the use of GC in intranasal vaccine applications. Follow-up gene expression profiling in this study hoped to provide insight into the intranasal mechanism by performing

bulk-RNA analysis on GC-treated nasal lymphoid tissue. There was a lack of organized results in the experiment (as seen in **Figure 18** and **Figure 20**), but this does not rule out the approach. Rather, it makes room for future optimization, particularly in the methods of homogenization.

Overall, this study provided valuable, significant evidence of the GC-induced type I interferon response and began optimization on methods for determining the mechanism by which this response occurred.

4.2 Future Directions

4.2.1 IVIS study

The immediate direction to take in building upon this study is performing the protocol with larger groups, as mentioned. Increasing group size with the improved injection protocol will provide greater statistical significance to the trend shown in this study. Additionally, further exploration of the adverse reaction observed, and subsequent optimization of the subcutaneous injection volume is necessary to eliminate variance and ensure reproducibility.

4.2.2 Homogenization method

As previously discussed, the main hypothesis for the variable results of this experiment is centered on the tissue homogenization method, so future studies will aim to optimize this for the production of significant immune results. This may entail optimization of the bead-beating method or another method entirely, as discussed above. Once the homogenization is shown to produce viable and representative nucleic acid content, other experiments may build upon the results that should be produced. First, single cell sequencing in addition to bulk sequencing may provide even more specific insight into immune interactions (Want, 2021). Future studies may survey a different tissue in the downstream of the reaction, for example lung tissue. Furthermore,

rather than bulk tissue assessment, cell-specific lysis could provide pinpointed interaction details. The bulk sequencing could first provide insight into which cells to isolate. Lastly, once GC sole effects are uncovered, future studies could perform this analysis after GC administered with another inoculation, as mentioned in the discussion. To specifically relate this back to the overall work of the lab, the additional inoculation could be with cancer cells prior to and after LIT treatment.

4.2.3 Studies for future applications of GC

Future studies utilizing the IVIS imaging modality hold promise in the monitoring of tumor progression as well (Albert Einstein College of Medicine, 2024). Learned protocols and imaging optimizations will benefit the future of the lab in endeavors such as these. Imaging of mammary tumor progression using the IVIS has already been done preliminarily (Lim, 2009). That study tagged tumor cells to express luciferase fluorescence. Combined with the reporter mouse model, both interferon DsRed signal and tumor luciferase signal could be measured, as the IVIS machine can measure multiple wavelengths (Caliper Life Sciences, 2024). This would allow comparison of the progression of the tumor size with progression of the immune response upon GC treatment. Furthermore, a better understanding of the optimizations of the RNA sequencing protocol can lead into the improvement of LIT as well. Using single-cell sequencing for tumor environment analysis during the tumor growth progression and treatment application could provide a whole new understanding of the immune and cell-to-cell interactions (Yu e. a., 2021). This deeper level of understanding only stands to benefit the lab by allowing improvements to the established use in cancer therapy.

Additionally, future studies will aim to prove the drug functionality for expansion to the use in other disease treatment types. As referenced and as shown in Appendix D: Previous

COVID survival study with GC, GC has reduced mortality in COVID studies. Thus, by understanding GC's mechanism in the intranasal cavity, future studies will also be able to find ways to expand GC's use into applications such as a COVID vaccine.

Bibliography

A Nacer, D. C. (2014). Imaging murine NALT following intranasal immunization with flagellin-modified circumsporozoite protein malaria vaccines. *Mucosal Immunology*, 304-314.

Agostino, e. a. (2022). Protocol for isolation and characterization of lung tissue resident memory T cells and airway trained innate immunity after intranasal vaccination in mice. *STAR Protocols*.

Albert Einstein College of Medicine. (2024). *In Vivo Imaging System (IVIS)*. Retrieved from Shared Facilities & Cores: https://einsteinmed.edu/research/shared-facilities/cores/77/in-vivo-imaging-system-ivis/#:~:text=The%20IVIS%20facility%20provides%20access,or%20far%2Dred%20fluorescent%20probes.

Bittner-Eddy, P. D. (2017). Discriminating between Interstitital and Circulating Leukocytes in Tissues of the Murine Oral Mucosa Avoiding Nasal-Associated Lymphoid Tissue Contamination. *Frontiers in Immunology*, 1398.

Caliper Life Sciences. (2024). *IVIS Spectrum: Advanced Small Animal Imaging of Fluorescent and Bioluminescent Probe.* Retrieved from iLab Solutions: https://content.ilabsolutions.com/wp-content/uploads/2014/11/IVIS-Spectrum-Advanced-Training-Presentation.pdf

Carroll, e. a. (2016). Th Vaccine Adjuvant Chitosan Promotes Cellular Immunity vis DNA Sensor cGAS-STING-Dependent Induction of Type I Interferons. *Immunity*, 597-608.

CD Genomics. (2024). *Bulk RNA Sequencing vs. Single Cell RNA Sequencing*. Retrieved from CD Genomics - RNA solutions: https://rna.cd-genomics.com/resource/bulk-rna-vs-single-cell-rna-seq.html

CDC. (2022, Sep 27). *Adjuvants and Vaccines*. Retrieved from CDC: https://www.cdc.gov/vaccinesafety/concerns/adjuvants.html

Cho, K. a. (2022). The Evasion Mechanisms of Cancer Immunity and Drug Intervention in the Tumor Microenvironment. *Frontiers in pharmacology*.

Cisney, F. H. (2012). Examining the role of nasopharymgeal-associated lymphoreticular tissue (NALT) in mouse responses to vaccines. *JoVE*, 3960.

Coates, e. a. (2023). Temporal profiling of human lymphoid tissues reveals coordinated defence to viral challenge. *BioRxiv*.

Cool, e. a. (2013). Comparison of In Vivo Optical Systems for Bioluminescence and Fluorescence Imaging. *Journal of Fluorescence*, 909-920.

Debertin, e. a. (2003). Nasal-associated lymphoid tissue (NALT): frequency and localization in young children. *Clinical and experimental immunology*, 503-507.

Dillekas, e. a. (2019). Are 90% of deaths from cancer caused by metastases? *Cancer medicine*, 5574-5576. Retrieved from https://www.ncbi.nlm.nih.gov/pmc/articles/PMC6745820/

Esha Bala, S. S. (2019). Ch 25. In *Natural Polysaccharides in Drug Delivery and Biomedical Applications* (pp. 567-588). Academic Press.

Fordyce, K. D. (2013). Long-term RNA persistence in postmortem contexts. *Investigative Genetics*, 7.

Hegenbarth, e. a. (2022). Perspectives on Bulk-Tissue RNA Sequencing and Single-Cell RNA Sequencing for Cardiac Transcriptomics. *Molecuar Medicine for Cardiology*.

Hoover, e. a. (2022). A novel biopolymer synergizes type I IFN and IL-1β production through STING. *bioRxiv*.

Hylander, R. a. (2022). Using Mice to Model Human Disease: Understanding the Roles of Baseline Housing-Induced and Experimentally Imposed Stresses in Animal Welfare and Experimental Reproducibility. *Animals: an open access journal from MDPI*, 371.

Illumina. (2024). *Study gene expression using RNA sequencing*. Retrieved from Illumina.com: https://www.illumina.com/techniques/sequencing/rna-sequencing.html

Jackson Laboratory. (2024). *069613 - M1Red Strain Details*. Retrieved from The Jackson Laboratory: https://www.jax.org/strain/037280

Jackson Laboratory. (n.d.). *C57BL/6-Tg(Irgm1-DsRed2)1Nci/Mmjax*. Retrieved from The Jackson Laboratory: https://www.jax.org/strain/037280

JoVE Journal. (2012). *Examining the role of NALT in mouse reponses to vaccines*. Retrieved from JoVE Journal: Immunology and Infection: https://app.jove.com/v/3960/examining-the-role-of-nasopharyngeal-associated-lymphoreticular-tissue-nalt-in-mouse-responses-to-vaccines

Kang, e. a. (2013). Characteristics of nasal-associated lymphoid tissue (NALT) and nasal absorption capacity in chicken. *PloS one*.

Lei, e. a. (2020). Activation and evasion of type I interferon responses by SARS-CoV-2. *Nature communications*.

Li, e. a. (2011). Preliminary safety and efficacy results of laser immunotherapy for the treatment of metastatic breast cancer patients. *Photochemical * photobiological sciences: Official journal of the European Photochemistry Association and the European Society for Photobiology*, 817-821.

Lim, e. a. (2009). In vivo Bioluminescent Imaging of Mammary Tumors Using IVIS Spectrum. *JoVE Journal of Biology*.

Liu, e. a. (2022). Antigen presentation and interferon signatures in B cells driven by localized ablative cancer immunotherapy correlate with extended survival. *Theranostics*, 639-656.

Love, A. K. (2015). RNA-seq workflow: gene-level exploratory analysis and differential expression. *F1000Research*, 1070.

McNab, e. a. (2015). Type I interferons in infectious disease. *Nature Reviews Immunology*, 87-103.

Mushegian, G. &. (2010). Measuring gene expression divergence: the distance to keep. *Biology direct*, 51.

Naylor, e. a. (2006). In situ photoimmunotherapy: a tumor-directed treatment for melanoma. *British Journal of Dermatology*, 1287-1292.

Nelson, S. A. (2021). Potentiating Lung Mucosal Immunity Through Intranasal Vaccination. *Frontieres in Immunology*, 808527.

NIH. (2021, October 11). *What is Cancer?* Retrieved from National Cancer Institute: https://www.cancer.gov/about-cancer/understanding/what-is-cancer

PennState: Huck Institutes of the Life Sciences. (2024). *RNA-seq Sample Guidelines*. Retrieved from Penn State University: https://www.huck.psu.edu/core-facilities/genomics-core-facility/sample-recommendations/rna-seq-sample-guidelines#:~:text=We%20not%20only%20like%20to,of%20a%20group%20of%20samples.

Romero, e. a. (2014). RNA-seq: impact of RNA degradation on transcript quantification. *BMC Biology*.

Shemesh, e. a. (2021). SARS-CoV-2 suppresses IFNβ production mediated by NSP1, 5, 6, 15, ORF6 and ORF7b but does not suppress the effects of added interferon. *PLOS Pathogens*.

Shim, e. a. (2020). Induction of systemic immunity through nasal-associated lymphoid tissue (NALT) of mice intranasally immunized with Brucella abortus malate dehydrogenase-loaded chitosan nanoparticles. *PloS one*.

Song, e. a. (2009). Glycated chitosan as a new non-toxic immunological stimulant. *Immunopharmacology and immunotoxicology*, 202-208.

Stetson, e. a. (2006). Type I interferons in host defense. *Immunity*, 373-381.

Stifter, e. a. (2019). Visualizing the Selectivity and Dynamics of Interferno Signaling In Vivo. *Cell reports*, 3539-3550.

Taylor, B. (n.d.). *In Vivo Imaging: IVIS Spectrum.* Retrieved from iLab Solutions: https://content.ilabsolutions.com/wp-content/uploads/2014/11/IVIS-Spectrum-Basic-Training-Presentation.pdf

Truett, e. a. (2000). NaOH extrction (quick dirty DNA preparation). *Biotechniques*, 52-54.

UT Southwestern Medical Center. (2022). *IVIS Spectrum (Bioluminescence and Fluorescence)*. Retrieved from Small Animal Imaging Resource: https://www.utsouthwestern.edu/research/core-facilities/sair/equipment/ivis-spectrum.html#:~:text=IVIS%20Spectrum%20(Bioluminescence%20and%20Fluorescence,expression%20patterns%20in%20living%20animals.

Vatner, e. a. (2019). STING, DCs, and the link between innate and adaptive tumor immunity. *Molecular Immunology*, 13-23.

Wang, e. a. (2009). RNA-Seq: a revolutionary tool for transcriptomics. *Nature reviews: Genetics*, 57-63.

Want, L. a. (2021). From bulk, single-cell to spatial RNA sequencing. *International Journal of Oral Science*.

Xitvogel, e. a. (2015). Type I interferons in anticancer immunity. *Nature eviews Immunology*, 405-414.

Yu, e. a. (2021). Statistical and Bioinformatics Analysis of Data from Bulk and Single-Cell RNA Sequencing Experiments. *Methods in Molecular Biology*, 143-175.

Yu, R. e. (2022). Type I interferon-mediated tumor immunity and its role in immunotherapy. *Cellular and Molecular Life Sciences*, 191.

Yu, X. e. (2021). Statistical and Bioinformatics Analysis of Data from Bulk and Single-Cell RNA Sequencing Experiments. *Methods in molecular biology*, 143-175.

Zaman, e. a. (2012). Strategies for intranasal delivery of vaccines. *Drug Delivery Translational Research*, 100-109.

Zhao, e. a. (2018). Biomedical Applications of Chitosan and its Derivative Nanoparticles. *Polymers*, 462.

Zhou. (2018). Local Phototherapy Synergizes with Immunoadjuvant for Treatment of Pancreatic Cancer through Induced Immunogenic Tumor Vaccine. *Clinical Cancer Research*, 5335-5346.

Zhou, e. a. (2015). InCVAX – A novel strategy for treatment of late-stage, metastatic cancers through photoimmunotherapy induced tumor-specific immunity. *Cancer Letters*, 169-177.

Supplemental Materials

Appendix A: IVIS Adverse Reactions

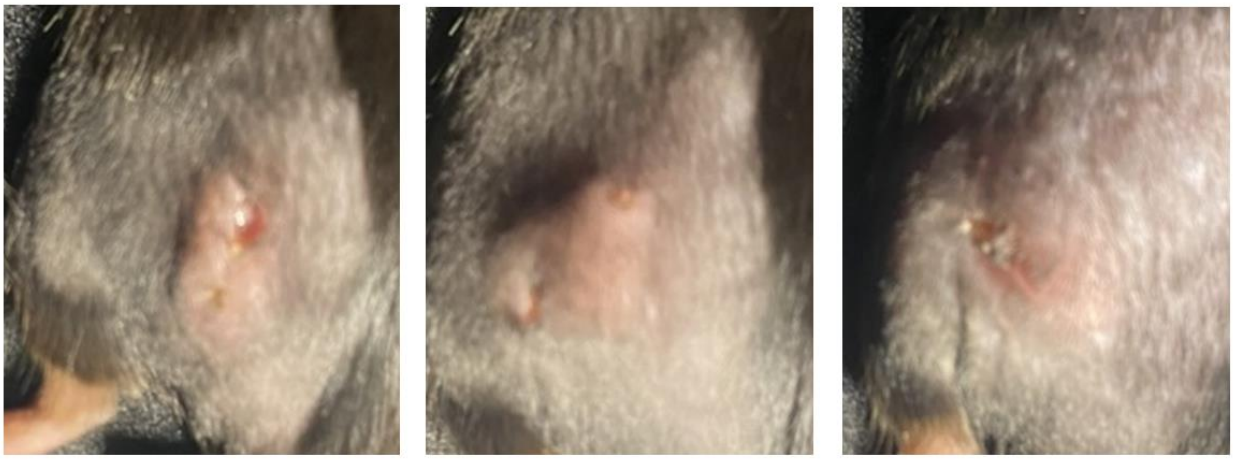

Figure 22: GC study adverse effects. *Adverse effects involving necrosis around the injection site for subcutaneous GC vaccinations in the IVIS study discussed in Chapter 2. Pictures taken 10 days post-drug-administration.*

Appendix B: Previous RNA Sequencing

"**Bone Marrow-Derived Dendritic Cell Cultures**

Bone marrow was isolated from 8 to 12-week-old male or female [WT mice]. Briefly, the animals were euthanized according IACUC approved protocols. The hind legs were removed and separated from the muscles and sinew. The heads of the bones were removed and 1x PBS was pushed through the bones using a 25-gauge needle and a 1ml syringe. The red blood cells were lysed, and cell were resuspended in RPMI containing 20% heat inactivated fetal calf serum, pen/strep, and β-mercaptoethanol. About 5×10^6 bone marrow cells were plated into 100mm non-tissue culture treated plates containing 20ng/ml GMCSF (Biolegend, Cat# 640920). On day 3 5ml of fresh media containing 20ng/ml of GMCSF was added to the cultures. On day 6 non-

adherent cells were collected and medium was removed and replaced with fresh RPMI containing 20ng/ml GMCSF and placed back into the 100mm plate. On day 7 the nonadherent BMDCs were collected for stimulation.

BMDC Activation

BMDCs were stimulated with GC or 2'3-cGAMP (InvivoGen, Cat# tlrl-nacga23-1) for 0-24 hours prior to ELISA or flow cytometry. About 10^6 cells/ml BMDCs were plated into a non-tissue culture treated 96 well round bottom plate and then stimulated with 0.08-16μg/ml GC. For 2'3-cGAMP stimulation, 200ng of 2'3-cGAMP was first encapsulated into viromer green transfection reagent (Origene, Cat# TT100301) according to the manufacturer's instructions prior to incubation with BMDCs.

VX765 was purchased from InvivoGen (Cat# inh-vx765i-1) and used at a concentration of 10μM. BMDCs were pre-incubated for 30 minutes with VX765 prior to the addition of GC. Bafilomycin A was purchased from InvivoGen (Cat# tlrl-baf1) and used at a concentration of 100nM. BMDCs were pre-incubated for 30 minutes with bafilomycin A prior to the addition of GC. GSK'872 was purchased from Millipore Sigma (Cat# 530389) and used at a concentration of 3μM. BMDCs were pre-incubated for 45 minutes with GSK'872 prior to the addition of GC.

RNA-Sequencing

BMDCs were cultured for 24 hours, then harvested and stained with ghost dye BV510 for viability and CD11b APC-Cy7 and CD11c FITC. Live CD11b+CD11c+ BMDCs were sorted on the BD FACS ARIA. RNA was isolated from the sorted BMDCs using the Quick-RNA microprep kit purchased from Zymo Research (Cat# R1050). RNA was isolated according to the manufacturer's protocol. For sequencing the 20M reads mRNA prep and sequencing service was performed for preparation of the RNA for NovaSeq PE150 reads on the NovaSeq6000.

Bioinformatics analysis (Quality control, read trimming, mapping to genome, and identification of DEGs)

A quality check for the raw sequencing data was conducted using *FastQC* (v0.11.9) to detect common issues in RNA-Seq data. The reads were then trimmed with *Trimmomatic* (v0.39) to remove low quality bases(*51*). The quality of the reads was re-evaluated with *FastQC* after this step to validate the quality improvements. The RNA-seq reads from each sample were mapped to the mouse mm10 genome assembly using the *HISAT2. Samtools* was used to manipulate the *HISAT2* generated SAM files into BAM files(*52*). *FeatureCounts* program from *Subread* package was used to count mapped RNAseq reads for genomic features(*53*). *DESeq2* was used for differential expressed genes (DEG) analysis based on the negative binomial distribution. The resulting P-values were adjusted using the Benjamini and Hochberg's approach for controlling the false discovery rate. Genes with an adjusted P-value (P adj) < 0.05 as determined by *DESeq2* were assigned as differentially expressed. Gene ontology (GO) analysis of DEG was performed using *clusterProfiler*(*54*)." (Hoover, 2022)

Appendix C: IVIS Optimization

C1: Chlorophyll Free Diet

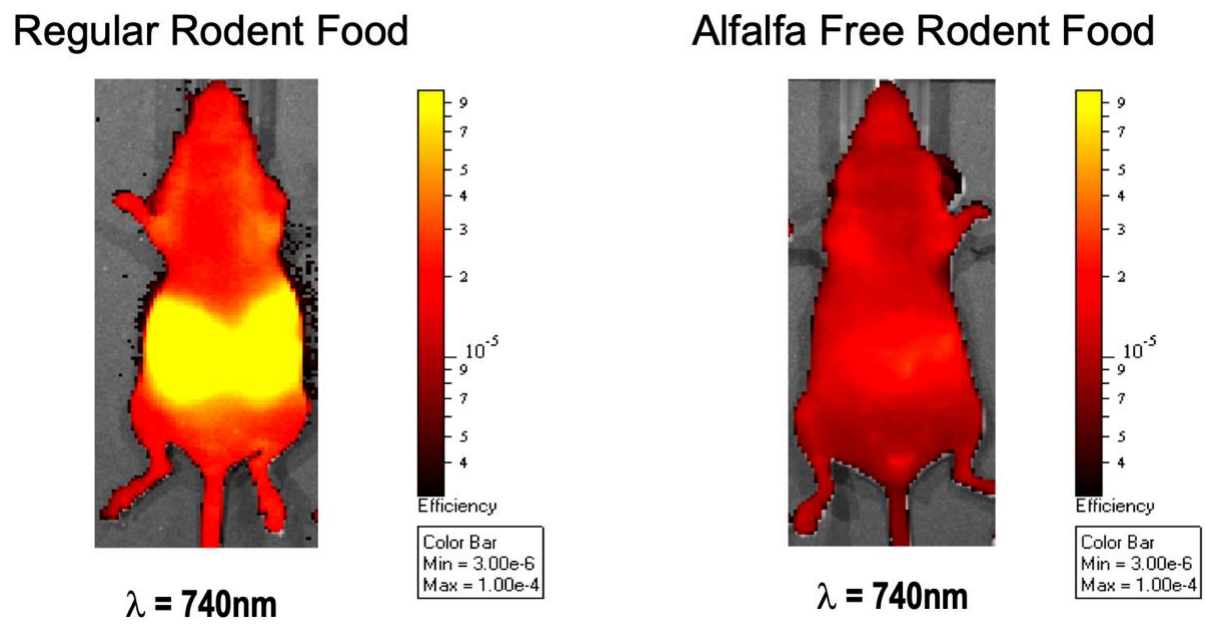

Figure 23: Difference in baseline fluorescence readings made by diet change. *This figure shows two images with the same fluorescence scale to show the difference on fluorescence signal made by alfalfa in the mouse's diet. The special diet reduces background noise (Taylor).*

C2: IVIS Field of Views

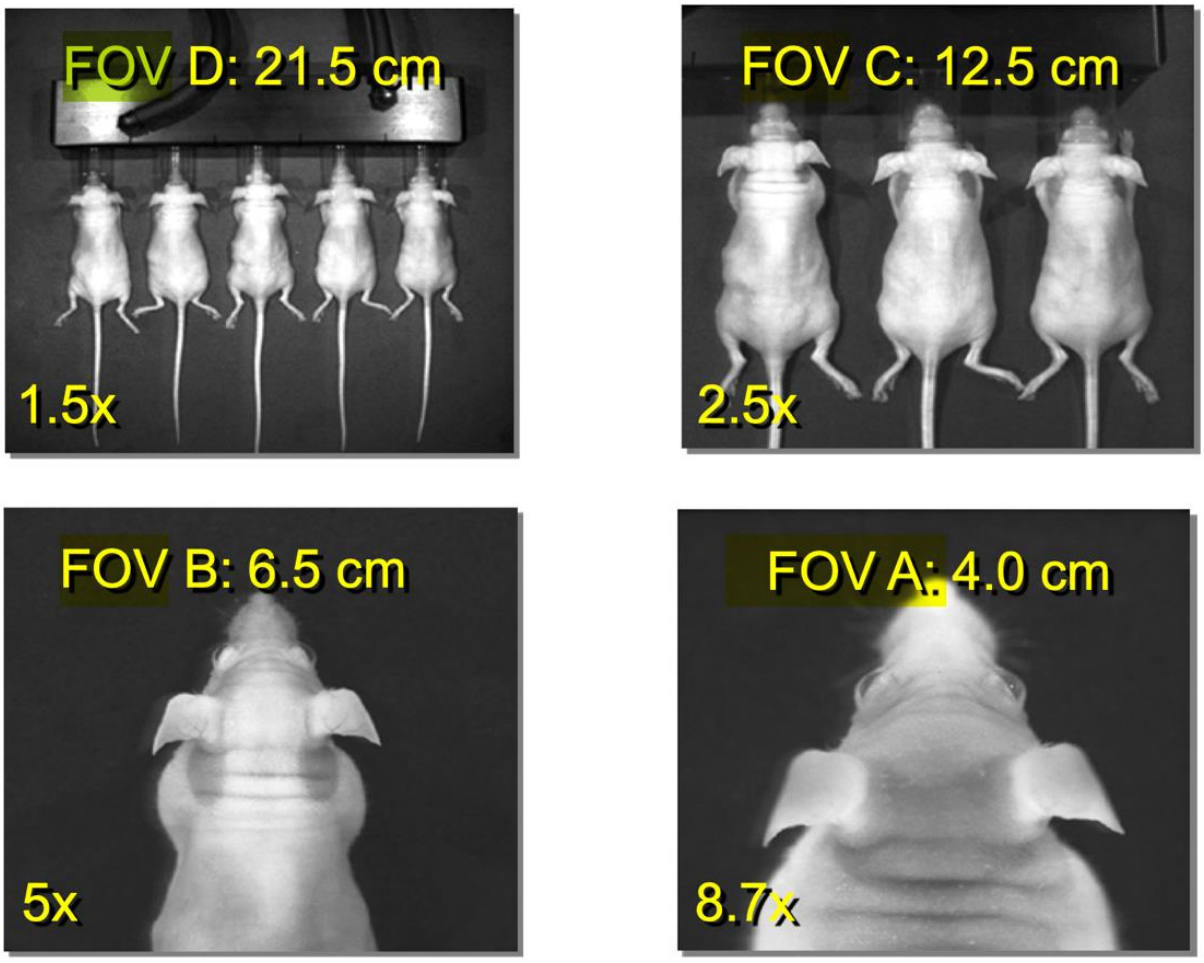

Figure 24: Field of view options in IVIS Spectrum imaging. *This image shows the different levels of field of view that are possible for imaging on the IVIS Spectrum CT machine. Different FOVs pose different advantages, e.g., FOV D can image more mice but has a farther distance for acquisition (Taylor).*

C3: Initial Round Relevant Results

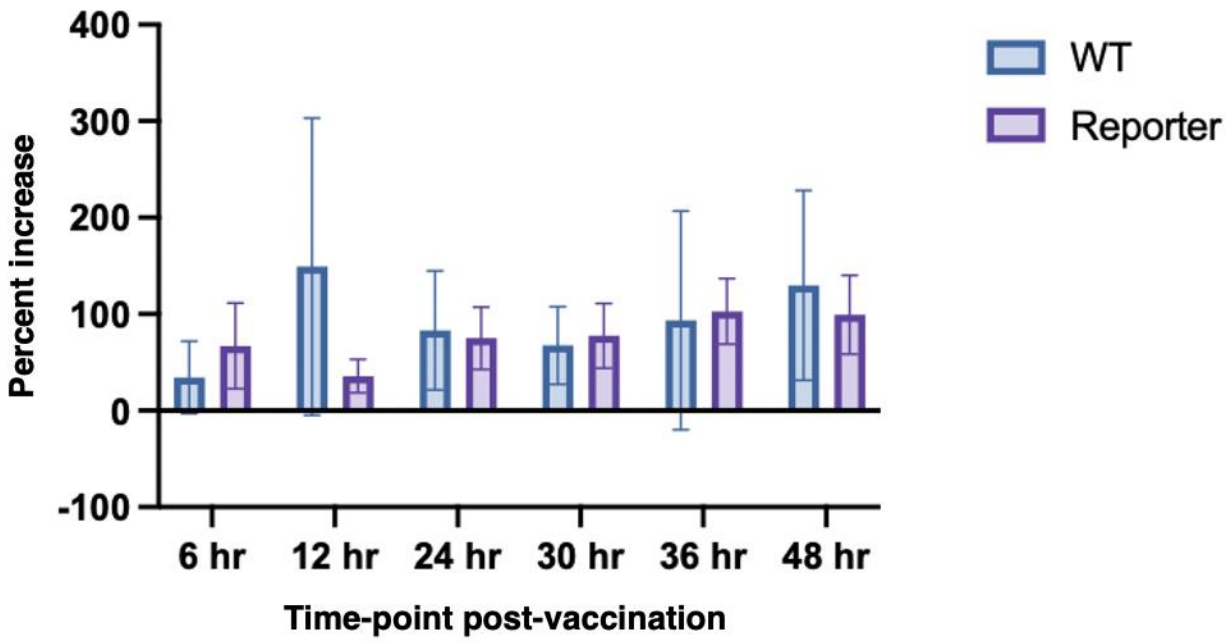

Figure 25: Preliminary subcutaneous results for percent increase in total radiant efficiency after GC administration. *Grouped bar graph depicting the percent change in total radiant efficiency measurements, as normalized to the background signal, in the local area after subcutaneous GC injection. This experiment was in the first round of IVIS imaging, done with only a 20µL injection volume, with WT mice as the control and IFN reporter mice as the test, both with GC treatment.*

Figure 25 shows the results of the first IVIS imaging round in the local subcutaneous area after GC injection. In this study, a volume of 20µL was used in an attempt to level out effects between the intranasal and subcutaneous injections (i.e., having both at the same volume). However, as can be seen in this figure, there is no visible trend and no statistically significant results from this study. Because of this, a larger volume was adopted for future trials.

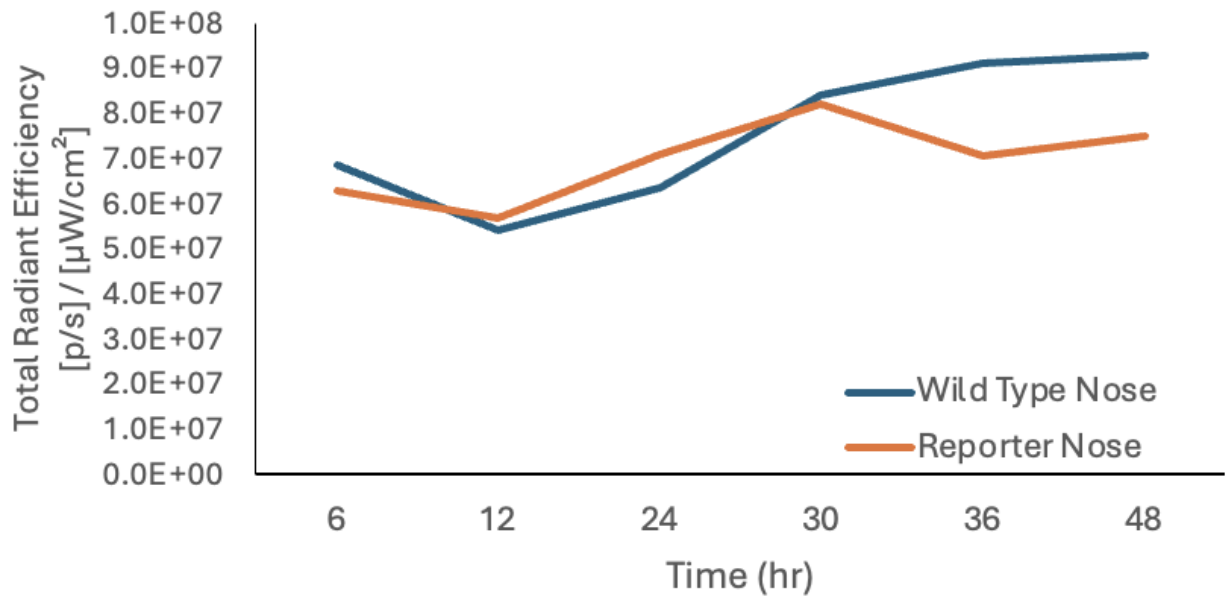

Figure 26: Preliminary intranasal results for raw total radiant efficiency counts after GC administration. *Line graph depicting the changes in total radiant efficiency measurements after intranasal vaccination with GC. This experiment was one of the primarily run rounds set for optimization and preliminary results. The difference between the two groups is essentially insignificant at all time points.*

Figure 26 shows the results of one of the preliminary intranasal vaccination studies. No significant results were seen, so a more careful vaccination method was employed, as discussed in 2.3.1. Intranasal vaccination. It had been hypothesized that perhaps the GC solution was not experiencing proper uptake into the mouse's nasal cavity, thus the lack of response. (In some of the mice, there was visual evidence of liquid on the floor of the recovery chamber (where the mouse is placed after the procedure), so this was basis for the development of a more careful protocol.)

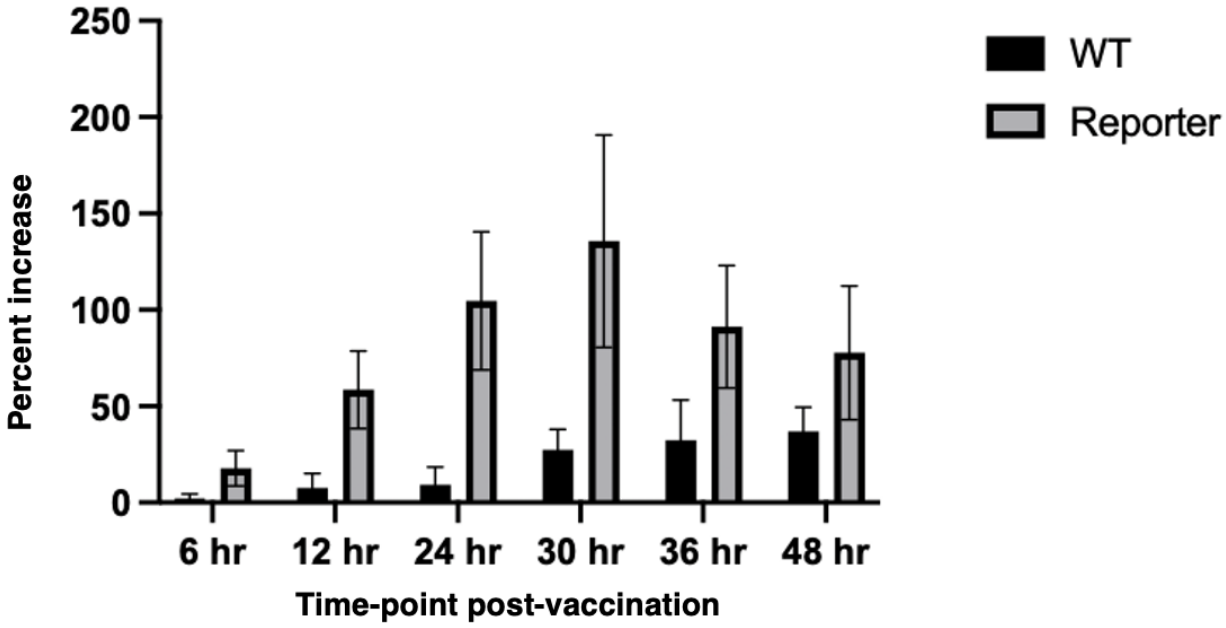

Figure 27: Previous round of intranasal imaging percentage increase in total radiant efficiency. *Bar graph depicting the percent increase in nasal fluorescent signal after intranasal vaccination with GC, as normalized to the background signal. This experiment was one of the primarily run rounds, where GC was administered to both WT (control) and IFN Reporter mice (test). No significance was found in comparisons between time points or between control and test.*

One of the earlier rounds of IVIS imaging was run with only 5 mice per group, as dictated by the number of reporter mice available in the facility at the time. While the graph in **Figure 27** does show an increase in the test group signal, there was no statistical significance found. For this reason, test group size was increased. The 10-per-group done in the intranasal study results reported in the main body of this paper show similar increases with proven statistical significance (although doing 10 per group for subcutaneous injections was not possible at this time due to animal availability constraints).

Appendix D: Previous COVID survival study with GC

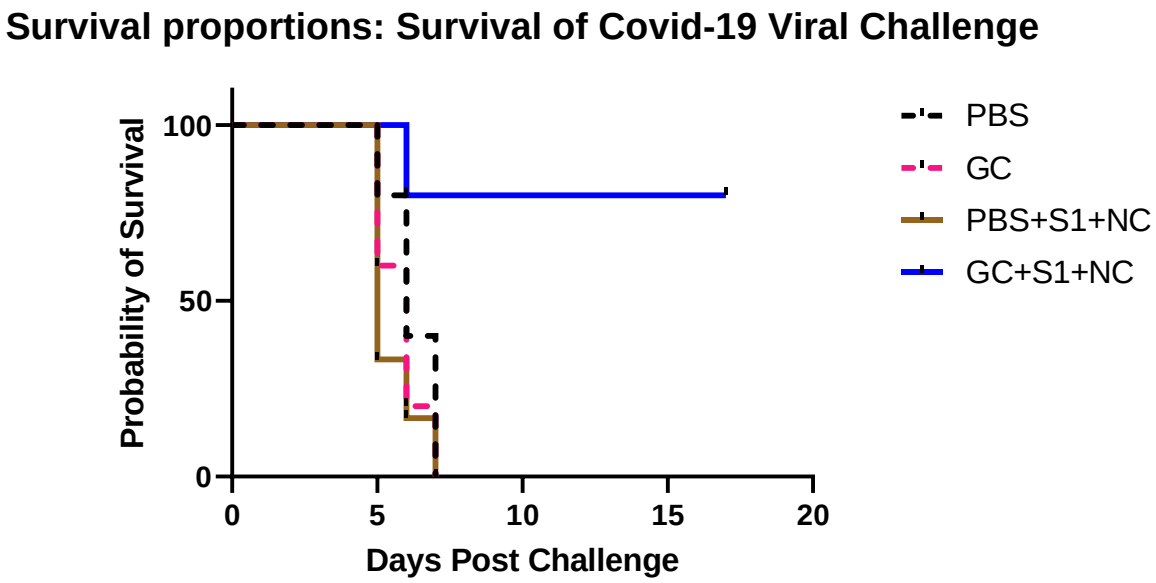

Figure 28: Previously run survival study of COVID treatment after GC and recombinant protein administration. *Graphs shows preliminary results of a previously run study in which GC was proven to reduce COVID mortality.*

Appendix E: Genotyping

E1: Custom Primers

Custom primers were ordered from Sigma-Aldrich. Sequences were as follows:

- Transgene 1: GGT GAT GTC CAG CTT GGA GT
- Transgene 2: CCC CGT AAT GCA GAA GAA GA
- Internal Positive Control Forward: CTA GGC CAC AGA ATT GAA AGA TCT
- Internal Positive Control Reverse: GTA GGT GGA AAT TCT AGC ATC ATC C

E2: Protocol

E2.1 DNA extraction

Protocol from (Truett, 2000). An ear punch from each mouse was used. An undiluted aliquot of the final product was taken for PCR.

E2.2 PCR

Materials:

DreamTaq Hot Start Green PCR Master Mix, (Thermo Fisher Scientific, CAT#K9021) was used.

Methods:

Recommendations from the DreamTaq user manual were employed.

Taq mix and primers were thawed completely and mixed. For each 50µL reaction, 25µL of taq mix, 2.5µL of each primer (one tube for transgene primers and one for IPC primers was used), 2µL of the DNA product, and 18µL of nuclease-free water were added to a thin-walled PCR tube. Samples were gently vortexed and centrifuged. For the thermal cycler run, the following optimizations were set against the user manual recommendations: 3 minute initial denaturation , melting temperature of 61℃, and a 10 minute final extension. (These settings will differ based on Taq mix and primers used.) The thermal cycler was run; at the end of the run, a 6µL portion of each sample was loaded directly into the agarose gel for the electrophoresis run.

E2.3 Electrophoresis

Materials:

Model D2 Horizontal Gel System from Thermo-Scientific was used for the electrophoresis run. Recommendations for running found in the user manual were used. 50 bp DNA Ladder from Thermo-Scientific was used for comparison (CAT#10416014).

Methods:

The following specifications were used for protocol adjustment.

- A 1.8% agarose gel was used, as recommended for the gene fragment size and as workable for the DNA ladder.
- 2.5µL ethidium bromide stock was added to the agarose gel mixture.
- The wet-loading method was employed.
- The gel was run at 90V for ~35 minutes (until the DNA had run the appropriate distance – 40 minutes was too long).